

CONTAINS PRIVILEGED INFORMATION
DO NOT RELEASE

**GEOMECHANICAL EVALUATION OF
NATURAL GAS STORAGE IN GALLERY NO. 2
SENECA LAKE STORAGE INCORPORATED
STORAGE PROJECT, NEW YORK**

Topical Report RSI-1574

by

Nils T. Skaug
Joel D. Nieland

RESPEC
P.O. Box 725
Rapid City, South Dakota 57709

RECEIVED
APR 25 '02
DIVISION OF
MINERAL RESOURCES

prepared for

PB-KBB, Inc.
P.O. Box 19672
Houston, Texas 77079

April 2002

EXECUTIVE SUMMARY

INTRODUCTION

In the fall of 2001, PB-KBB, Inc. engaged RESPEC to perform a geomechanical evaluation of a compressed natural gas storage project on the west shore of Seneca Lake near Watkins Glen, New York. Seneca Lake Storage Incorporated (SLSI) is developing the storage project, which involves the conversion of an existing gallery of solution-mined caverns owned by U.S. Salt. The gallery, designated as Gallery No. 2, was developed via Well No. 30 and Well No. 31 in a series of salt beds at a depth range of about [REDACTED] feet below the ground surface at Well No. 31.

1957
Well No. 30 was drilled in 1958 and Well No. 31 was drilled in 1961. Gallery No. 2 was used originally for brine production and was converted to LPG storage in 1964. Well No. 45 was drilled into Gallery No. 2 in 1968 with the intention of increasing storage capacity by lowering the propane-brine interface. LPG storage ceased and the gallery was filled with brine in 1984, and the three wells into the gallery were plugged in 1989 [Medley, 1993].

In 1996, RESPEC performed a geomechanical evaluation of Gallery No. 1 located on U.S. Salt property before it was converted to natural gas storage by New York State Electric and Gas Corporation (NYSEG) [Osnes and Eyermann, 1996]. Since then, natural gas has been successfully stored in Gallery No. 1. Gallery No. 1 is located about [REDACTED] east of Gallery No. 2. Given the close proximity of the two galleries, site-specific information and properties used in the 1996 study are used to the extent possible in this study. This report describes the methodology and results of the geomechanical analyses of Gallery No. 2.

TECHNICAL APPROACH

The objective of the geomechanical evaluation is to determine the operating pressure range in Gallery No. 2 during natural gas storage service that will ensure the structural stability of the salt and nonsalt strata surrounding the cavern and the gas containment capability of the cavern. The gallery is suitable for compressed natural gas service if the analysis determines that the gallery exhibits:

- Extremely limited dilation (microfracturing) in the surrounding salt.
- Sufficiently high factors of safety to preclude the possibility of shear failure in the surrounding nonsalt layers.
- Limited areas in which the least-compressive principal stresses approach the tensile strengths of the nonsalt and salt beds.

CONTAINS PRIVILEGED INFORMATION
DO NOT RELEASE

To achieve the objectives of this study, finite difference simulations are used to evaluate the stress states and the displacements in the surrounding rock of Gallery No. 2 before and during various gas storage cycles. In these cycles, the gas pressure is varied between the proposed minimum and maximum operating pressures to determine a pressure range that satisfies the four criteria listed at the beginning of this section. The proposed minimum and maximum wellhead pressures for Gallery No. 2 are [REDACTED] respectively.

MODELING RESULTS

The impact of converting Gallery No. 2 from its current brine-filled condition to gas storage service on surrounding caverns and surface conditions was evaluated. Finite difference simulations predicted that Gallery No. 2 is [REDACTED]. This conclusion is based on the [REDACTED]. The [REDACTED] caused by gas storage in Gallery No. 2 is [REDACTED].

The structural stability of Gallery No. 2 was assessed by examination of the finite difference modeling results. The modeling results were evaluated based on strength, creep, and dilation properties of the gallery's host formation. The stability evaluation included an assessment of the roof stability of the gallery and the potential for rock spalling from the sidewalls. These assessments are briefly summarized below.

The minimum factor of safety in the nonsalt roof rocks is [REDACTED] throughout the simulated gas storage. Potential for dilation (microfracturing) of salt in the roof was found to be [REDACTED] in the finite difference model. Thus the cavern roofs are [REDACTED].

The finite difference modeling results indicate that the potential for [REDACTED]

[REDACTED]

[REDACTED]

CONTAINS PRIVILEGED INFORMATION
DO NOT RELEASE

CONCLUSIONS

A comprehensive geomechanical analysis has been completed for the conversion of Gallery No. 2 to compressed natural gas storage service. The geomechanical analysis included:

- Development of the structural stratigraphy at the site based on existing literature and borehole geophysical logs.
- Development of cavern geometries based on sonar surveys.
- Characterization of rock properties.
- Characterization of the in situ temperature and stress states.
- Finite difference modeling of the initial cavern development, dewatering, and natural gas service.

The results of the geomechanical modeling have been evaluated using a set of performance criteria necessary to ensure safe and structurally stable gas containment in the gallery. The following performance criteria were established:

- Extremely limited dilation (microfracturing) in the surrounding salt.
- Sufficiently high factors of safety to preclude the possibility of shear failure in the surrounding nonsalt layers.
- Limited areas in which the least-compressive principal stresses approach the tensile strengths of the nonsalt and salt beds.
- Acceptable rates of closure and surface subsidence.

[REDACTED] Salt dilation and subsequent spalling is [REDACTED]
[REDACTED] Shear failure of the nonsalt strata, particularly [REDACTED]
[REDACTED] The minimum factor of safety in the roof bedding is [REDACTED] at the minimum gas pressure. [REDACTED]

[REDACTED]
[REDACTED]
[REDACTED] Converting Gallery No. 2 from its brine-filled condition to natural gas storage [REDACTED]
[REDACTED]

Operation of Gallery No. 2 in compressed natural gas service can [REDACTED]
[REDACTED]
[REDACTED]

Gallery No. 1 is [REDACTED]. Previous geomechanical analyses [Osnes and Eyermann, 1996] indicated that natural gas storage in

CONTAINS PRIVILEGED INFORMATION
DO NOT RELEASE

[REDACTED] Natural gas has been successfully stored in Gallery No. 1 since that study. The current analyses indicate that the structural integrity of Gallery No. 1 [REDACTED]
Also, because the [REDACTED]
[REDACTED]

TABLE OF CONTENTS

1.0 INTRODUCTION.....	1
1.1 BACKGROUND	1
1.2 SCOPE AND OBJECTIVES OF GEOMECHANICAL ANALYSES.....	1
1.3 REPORT ORGANIZATION.....	3
2.0 DESCRIPTION OF GALLERY NO. 2.....	4
2.1 THE CAVERN FIELD NEAR WATKINS GLEN, NEW YORK.....	4
2.2 THE DEVELOPMENT AND HISTORY OF GALLERY NO. 2.....	6
3.0 TECHNICAL APPROACH	10
3.1 OVERVIEW OF THE APPROACH	10
3.2 STRATIGRAPHIC MODEL	11
3.3 MATERIAL PROPERTIES	16
3.3.1 Elastic Properties	16
3.3.2 Salt Creep Characterization.....	17
3.3.3 Salt and Nonsalt Strength.....	20
3.3.3.1 Salt Dilation Criterion.....	21
3.3.3.2 Shear Failure Criterion for Nonsalt Strata	23
3.3.3.3 Tensile Strength.....	25
3.4 IN SITU CONDITIONS.....	26
3.4.1 In Situ Stress Distribution	26
3.4.2 Geothermal Temperature Profile	26
3.5 PROPERTIES OF CAVERN FLUIDS.....	27
3.5.1 Natural Gas Properties.....	27
3.5.2 Brine Properties	28
3.6 NUMERICAL MODELING.....	28
3.6.1 Finite Difference Program	28
3.6.2 Finite Difference Model.....	29
3.6.3 Subsidence Simulation Program.....	34
4.0 CAVERN OPERATING PRESSURES	35
4.1 BRINE AND LPG STORAGE	35
4.2 DEWATERING - CONVERSION TO NATURAL GAS STORAGE.....	35
4.3 GAS STORAGE	36
5.0 MODELING RESULTS	41
5.1 INTERACTION BETWEEN GALLERY NO. 1 AND GALLERY NO. 2	41

TABLE OF CONTENTS
(Continued)

5.2	BRINE AND LPG STORAGE.....	43
5.3	DEWATERING - CONVERSION TO NATURAL GAS STORAGE	47
5.4	NATURAL GAS STORAGE SCENARIOS	49
5.5	CAVERN CLOSURE AND SUBSIDENCE RATES DURING GAS STORAGE.....	62
6.0	SUMMARY	65
7.0	CONCLUSIONS	67
8.0	REFERENCES	69

LIST OF TABLES

TABLE	PAGE
3-1 Stratigraphy Modeled in the Gallery No. 2 Simulations	15
3-2 Stratigraphy Within Syracuse Formation Modeled in the Gallery No. 2 Simulations.....	15
3-3 Elastic Properties Used to Represent the Geologic Units in the Stratigraphic Model.....	18
3-4 Creep Parameters for Salt	20
4-1 Cavern Operating Pressures for Gallery No. 1 and Gallery No. 2	37

LIST OF FIGURES

FIGURE	PAGE
2-1 Plan View of the Watkins Glen Cavern Field	5
2-2 East-West Cross Sections of the Well No. 30 and Well No. 31 Caverns as Indicated by Most Recent Sonar Caliper Surveys	7
2-3 North-South Cross Sections of the Well No. 30 and Well No. 31 Caverns as Indicated by Most Recent Sonar Caliper Surveys	9
3-1 Stratigraphy of the Syracuse Formation Based on Core Log From Well No. 27 and Open-Hole Logs From Well No. 31	12
3-2 Stratigraphy of the Syracuse Formation Used in the Finite Difference Model	14
3-3 Steady-State Creep Rates for the Munson-Dawson Model and the Two-Component Power Law	19
3-4 Dilation Response of Salt From Well No. 58 and Well No. 59 Based on Creep and Constant Mean Stress Tests	22
3-5 Failure Criterion for the Nonsalt Strata Based on Triaxial Compression Tests of Camillus Formation Specimens From Well No. 59	24
3-6 Plan View of FLAC ^{3D} Model and Maximum Radius Outlines	30
3-7 East-West Cross Section Through the Stratigraphy and the Projection of the Caverns Included in the Model	32
3-8 Various Views of the FLAC ^{3D} Model	33
4-1 Minimum/Maximum Pressure Scenarios Evaluated for Gallery No. 1 and Gallery No. 2	38
4-2 Simulated Annual Pressure Cycles for Gallery No. 1 and Gallery No. 2	39
5-1 Maximum Change in Principal Stress at the Cavern Surface of Gallery No. 2 With Gallery No. 1 at [REDACTED] Pressure and Gallery No. 2 at [REDACTED] Pressure	42
5-2 Damage Potential Predicted on the Surfaces of Gallery No. 1 and Gallery No. 2 After [REDACTED] of Brine Production and LPG Storage	44
5-3 Northern View of Factors of Safety Predicted in the Nonsalt Strata Around Gallery No. 1 and Gallery No. 2 After [REDACTED] of Brine Production and LPG Storage	45
5-4 Southern View of Factors of Safety Predicted in the Nonsalt Strata Around Gallery No. 1 and Gallery No. [REDACTED] of Brine Production and LPG Storage	46
5-5 Regions of Tensile Fracturing Predicted During [REDACTED] of Brine Pressure	48
5-6 Damage Potential Predicted in the Salt Around Gallery No. 2 After [REDACTED] at Maximum Pressure	50

LIST OF FIGURES
(Continued)

FIGURE	PAGE
5-7 Northern View of Factors of Safety Predicted in the Nonsalt Strata Around Gallery No. 1 and Gallery No. 2 After [REDACTED] at Maximum Pressure.....	51
5-8 Southern View of Factors of Safety Predicted in the Nonsalt Strata Around Gallery No. 1 and Gallery No. 2 After [REDACTED] at Maximum Pressure.....	52
5-9 Damage Potential Predicted in the Salt Around Gallery No. 2 Immediately After Pressure Reduction to Minimum Pressure.....	54
5-10 Damage Potential Predicted in the Salt Around Gallery No. 2 After [REDACTED] at Minimum Pressure	55
5-11 Northern View of Factors of Safety Predicted in the Nonsalt Strata Around Gallery No. 1 and Gallery No. 2 Immediately After Pressure Reduction to Minimum Pressure	56
5-12 Southern View of Factors of Safety Predicted in the Nonsalt Strata Around Gallery No. 1 and Gallery No. 2 Immediately After Pressure Reduction to Minimum Pressure	57
5-13 Northern View of Factors of Safety Predicted in the Nonsalt Strata Around Gallery No. 1 and Gallery No. 2 After [REDACTED] at Minimum Pressure.....	58
5-14 Southern View of Factors of Safety Predicted in the Nonsalt Strata Around Gallery No. 1 and Gallery No. 2 After [REDACTED] at Minimum Pressure.....	59
5-15 Regions of Tensile Fracturing Predicted Immediately After Reducing Pressures in Gallery No. 1 and Gallery No. 2 to Minimum Pressure.....	60
5-16 Regions of Tensile Fracturing Predicted After [REDACTED] at Minimum Pressure for Gallery No. 1 and Gallery No. 2.....	61
5-17 Volumetric Closure During 5-Year Pressure Cycle.....	63

1.0 INTRODUCTION

1.1 BACKGROUND

In the fall of 2001, PB-KBB, Inc. engaged RESPEC to perform a geomechanical evaluation of a compressed natural gas storage project on the west shore of Seneca Lake near Watkins Glen, New York. Seneca Lake Storage Incorporated (SLSI) is developing the storage project, which involves the conversion of an existing gallery of solution-mined caverns owned by U.S. Salt. The gallery, designated as Gallery No. 2, was developed via Well No. 30 and Well No. 31 in a series of salt beds at a depth range of about [REDACTED] feet to [REDACTED] feet below the ground surface at Well No. 31.

Well No. 30 was drilled in 1958 and Well No. 31 was drilled in 1961. Gallery No. 2 was used originally for brine production and was converted to LPG storage in 1964. Well No. 45 was drilled into Gallery No. 2 in 1968 with the intention of increasing storage capacity by lowering the propane-brine interface. LPG storage ceased and the gallery was filled with brine in 1984, and the three wells into the gallery were plugged in 1989 [Medley, 1993].

In 1996, RESPEC performed a geomechanical evaluation of Gallery No. 1 located on U.S. Salt property before it was converted to natural gas storage by New York State Electric and Gas Corporation (NYSEG) [Osnes and Eyermann, 1996]. Since then, natural gas has been successfully stored in Gallery No. 1. Gallery No. 1 is located about [REDACTED] east of Gallery No. 2. Given the close proximity of the two galleries, site-specific information and properties used in the 1996 study are used to the extent possible in this study.

The geomechanical evaluation of Gallery No. 2 has three technical tasks:

- **Task 1** — Model Development Based on Facility, Geological, and Design Information
- **Task 2** — Geomechanical Modeling to Evaluate an Acceptable Operating Pressure Range
- **Task 3** — Reporting of Results to PB-KBB.

This report describes the methodology and results of the geomechanical analyses of Gallery No. 2.

1.2 SCOPE AND OBJECTIVES OF GEOMECHANICAL ANALYSES

The objective of the geomechanical evaluation is to determine the operating pressure range in Gallery No. 2 during natural gas storage service that will ensure the structural stability of the salt and nonsalt strata surrounding the cavern and the gas containment capability of the

CONTAINS PRIVILEGED INFORMATION
DO NOT RELEASE

cavern. The operating pressures for natural gas storage will be established while considering the following criteria:

- The recommended maximum and minimum operating pressures will not result in connectivity with adjacent caverns caused by tensile failure or hydraulic fracturing.
- The recommended minimum operating pressure will not result in dilation (microfracturing) of the salt or shear failure of the nonsalt units that could lead to spalling of the roof and/or walls of the cavern and subsequent damage to the well or hanging string.
- The recommended minimum operating pressure and the operating pressure cycle will not yield excessive cavern closure that could produce excessive subsidence and/or damage to adjacent caverns and well casings.

These items are evaluated in this study using three-dimensional, finite difference simulations of Gallery No. 2 to predict the time-dependent stress states and displacement fields in the strata surrounding the gallery. Given the close proximity of the galleries, Gallery No. 1 is included in the model. To approximate the current stress state, simulations of [REDACTED] of brine production, LPG storage, and brine storage are modeled. This is followed by various gas storage cycles, including cycles between the minimum and maximum operating pressures. The stress states predicted in the finite difference simulations are interpreted in terms of factors of safety against shear failure in the nonsalt strata and in terms of potentials for dilation (microfracturing) in the salt. The closure of the galleries is calculated directly in the finite difference code, and the associated surface subsidence is determined from the galleries' closure using a subsidence prediction program.

Besides the gas storage pressures, the structural and operational integrity of a natural gas storage cavern depends primarily on the following factors:

- Strength and deformation characteristics of the salt and nonsalt units surrounding and overlaying the cavern
- Preexisting in situ state of stress in the region
- Size and shape of the cavern
- Stratigraphy
- Proximity to and interaction with nearby caverns.

Material properties of the salt and shale overlying Gallery No. 1 were measured in RESPEC's rock mechanics laboratory [Pfeifle, 1996]. These properties were used in the model of Gallery No. 2. The remainder of the preceding factors had to be estimated to some degree or inferred from other measurements in the region. In developing these estimates and inferences, conservative yet reasonable quantities were selected to provide additional assurance that the

integrity of the storage gallery will not be compromised when operated within the range of storage pressures recommended in this geomechanical analysis.

1.3 REPORT ORGANIZATION

A brief description of Gallery No. 2 is provided in Chapter 2.0 of this report. Chapter 3.0 contains a detailed description of the technical approach used in the geomechanical analyses. Evaluation of the cavern operating pressures is presented in Chapter 4.0. Chapter 5.0 presents the results of the simulations of Gallery No. 2. A summary of the modeling results is presented in Chapter 6.0, and conclusions are given in Chapter 7.0. References cited in this report are listed in Chapter 8.0.

2.0 DESCRIPTION OF GALLERY NO. 2

2.1 THE CAVERN FIELD NEAR WATKINS GLEN, NEW YORK

Gallery No. 2 is located in a field of solution-mined caverns owned by U.S. Salt. The cavern field is located on the west shore of Lake Seneca near the lake's southern end and is approximately 4 miles north of the town of Watkins Glen in south-central New York. The field has been in brine production for over a century.

All of the caverns are located in the bedded salt deposits of the Syracuse Formation. Over the extent of the cavern field, the elevation of the top of the Syracuse Formation varies from about [REDACTED] feet above mean sea level (amsl) to [REDACTED] feet amsl [PB-KBB, Inc., 1995] (the ground elevation above Gallery No. 2 ranges from [REDACTED] feet amsl to [REDACTED] feet amsl). The Syracuse Formation is approximately [REDACTED] feet thick in the cavern field. The formation contains [REDACTED] geologic units that are designated the [REDACTED] Units from bottom to top, and each unit contains one or more salt beds.

Figure 2-1 shows a plan view of Gallery No. 2 and its relationship to other wells and caverns in the field. As indicated by the well locations in this figure, the gallery is partially surrounded by caverns, with no cavern development to the west of Gallery No. 2. Caverns developed from wells [REDACTED]. As the diameters of these caverns increased, they eventually coalesced with adjacent caverns to form galleries. These caverns generally penetrated less than 100 feet of the upper portion of the Syracuse Formation [Jacoby, 1962]. Beginning in the mid-1950s with Well No. 27 and Well No. 28, galleries of caverns were mined using multiwell methods by initially hydraulically fracturing between pairs of wells near the base of the Syracuse Formation. Solution mining progressed upward through the Syracuse Formation by allowing the nonsalt layers between salt beds to collapse into the underlying cavern, thereby exposing the overlying salt to solutioning.

Figure 2-1 does not show the interconnections between wells and the galleries of caverns that developed from these interconnections. [REDACTED]

[REDACTED] in the plan view shown in Figure 2-1, the web of unmined rock between [REDACTED] thick. To the east of Gallery No. 2, Gallery No. 1 was developed between Well No. 27 and Well No. 28 (Well No. 46 and Well No. 59 were subsequently drilled into the roof of Gallery No. 1). The web between Gallery No. 1 and Gallery No. 2 is about [REDACTED]

CONTAINS PRIVILEGED INFORMATION
DO NOT RELEASE

RSI-1300-02-001



Figure 2-1. Plan View of the Watkins Glen Cavern Field.

CONTAINS PRIVILEGED INFORMATION
DO NOT RELEASE

To the northeast of Gallery No. 2 is the North Gallery, which was formed by the [REDACTED]. Because the solution mining of these caverns was [REDACTED]. The small cavern at [REDACTED] to the [REDACTED] of Gallery [REDACTED] was developed near the [REDACTED]. The web between this cavern and Gallery No. 2 is about [REDACTED] thick. To the north of Gallery No. 1 [REDACTED]

2.2 THE DEVELOPMENT AND HISTORY OF GALLERY NO. 2

Gallery No. 2 was initially developed via a [REDACTED]. The elevations of the ground surface at these two wells are approximately [REDACTED] amsl and [REDACTED] amsl, respectively. The connection between the wells was [REDACTED] amsl [Jacoby, 1969] near the base of the Syracuse Formation in Unit D. The gallery was solution mined until 1964 when it was converted to LPG storage. Records indicate a total salt production of about [REDACTED] of salt from Gallery No. 2, with [REDACTED]. Dissolution of [REDACTED] of salt will produce a void volume of approximately [REDACTED] (bbls). [REDACTED]

LPG was stored in Gallery No. 2 for a 20-year period. About 800,000 bbls of propane were stored in the gallery during the 1970s. In 1968, Well No. 45 was drilled into the lower portion of the gallery with the intention of increasing storage capacity by lowering the propane-brine interface. [REDACTED]. The surface elevation of Well No. 45 is approximately 718 feet amsl. After the cessation of LPG storage operations in 1984, the three wells into the gallery were plugged in 1989.

The Well No. 30 cavern was last surveyed by sonar in December 1997, and the latest available sonar for Well No. 31 dates back to July 1978. Figure 2-2 shows the east-west cross sections of the sonars from Well No. 30 and Well No. 31 projected onto an east-west plane, together with the projected locations of Well No. 30, Well No. 31, and Well No. 45. The approximate elevation of the hydraulic fracture that initially connected between Well No. 30 and Well No. 31 is also shown.

Figure 2-2 indicates that only the [REDACTED]

CONTAINS PRIVILEGED INFORMATION
DO NOT RELEASE

RSI-1300-02-002

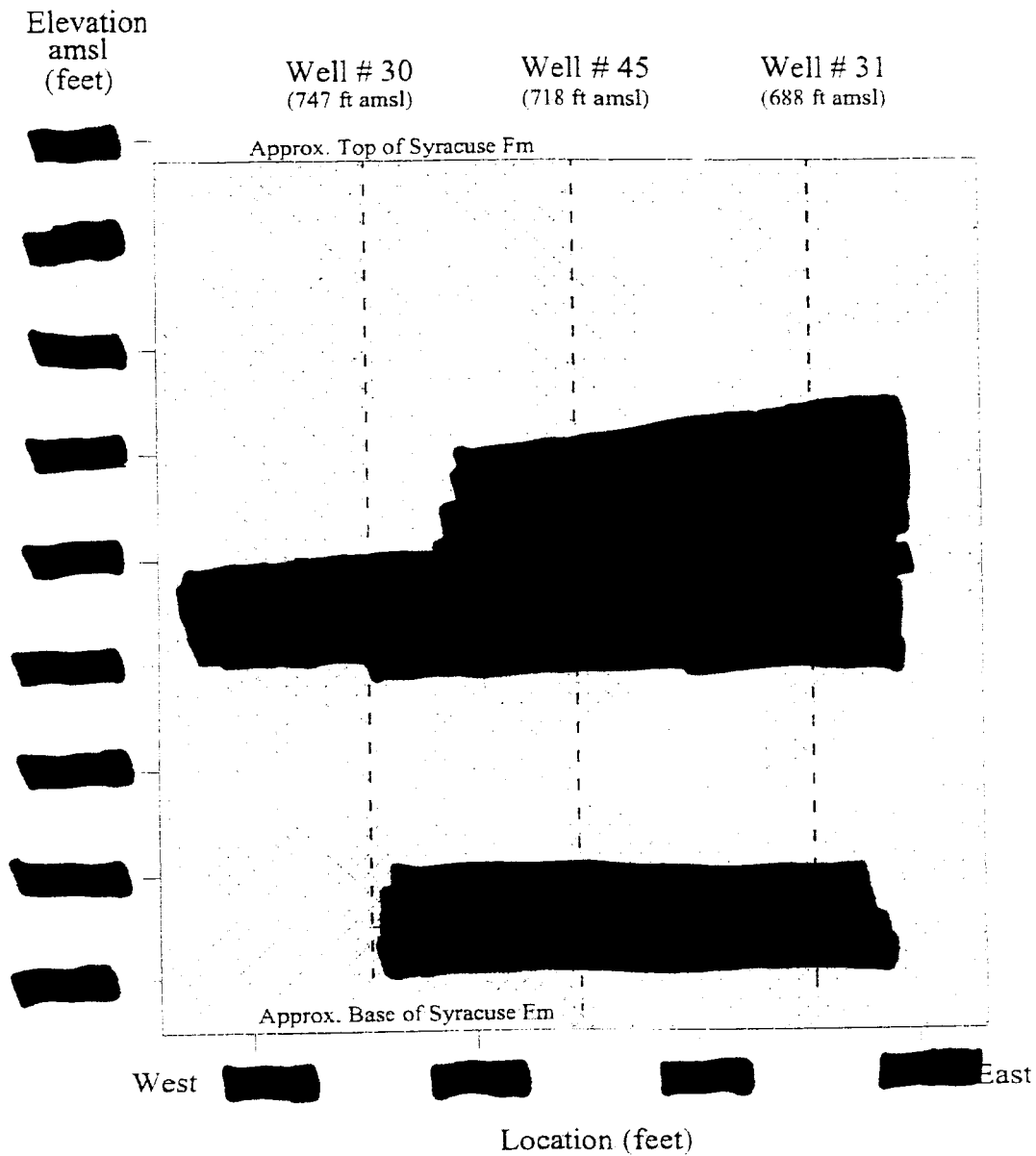


Figure 2-2. East-West Cross Sections of the Well No. 30 and Well No. 31 Caverns as Indicated by Most Recent Sonar Caliper Surveys.

CONTAINS PRIVILEGED INFORMATION
DO NOT RELEASE



Figure 2-3 shows the north-south sonar cross sections of the Well No. 30 cavern and Well No. 31 cavern projected onto the north-south plane. The projections of the wells and the approximate elevation of the hydraulic fracture that initially connected the wells are also included in the figure.

RSI-1300-02-003

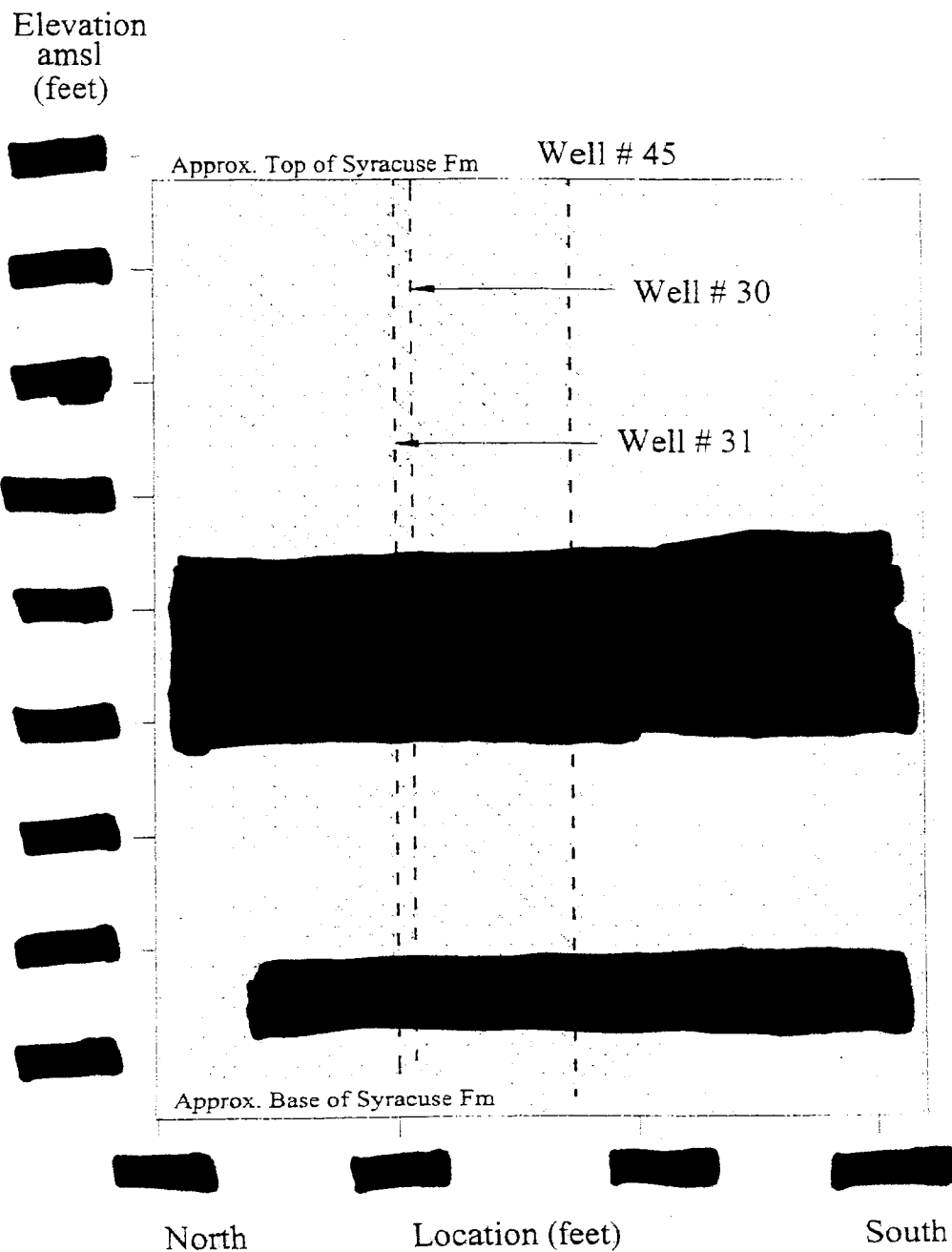


Figure 2-3. North-South Cross Sections of the Well No. 30 and Well No. 31 Caverns as Indicated by Most Recent Sonar Caliper Surveys.

3.0 TECHNICAL APPROACH

3.1 OVERVIEW OF THE APPROACH

The objective of the geomechanical evaluation is to determine the operating pressure range in Gallery No. 2 during natural gas storage service that will ensure the structural stability of the salt and nonsalt strata surrounding the cavern and the gas containment capability of the cavern. The gallery is suitable for compressed natural gas service if the analysis determines that the gallery exhibits:

- Extremely limited dilation (microfracturing) in the surrounding salt.
- Sufficiently high factors of safety to preclude the possibility of shear failure in the surrounding nonsalt layers.
- Limited areas in which the least-compressive principal stresses approach the tensile strengths of the nonsalt and salt beds.
- Acceptable rates of closure and surface subsidence.

The first three criteria are required to ensure the stability of the gallery and to prevent interconnection with adjacent caverns. The expected useful life of the gallery for natural gas storage is directly related to the fourth criterion.

The potential consequences associated with violating any of the first three criteria depend on the area in which a criterion is not satisfied. Areas along the surface of the gallery are of limited concern because a minor amount of roof and wall spalling can be tolerated without instability of the gallery or interconnection with adjacent caverns. Failures in areas above the roof of the gallery, especially near the casing seats, would have the most severe consequences. Hence, the failure criteria must be interpreted most conservatively in the areas overlying the gallery.

Extensive violation of the first two criteria in the webs between the gallery and adjacent caverns also could lead to instability of the gallery. Violation of the third criterion might result in the loss of containment of the natural gas. Gallery No. 1 is of special interest in contrast with the other caverns in the cavern field because [REDACTED] and its pressure varies as gas is injected or withdrawn. [REDACTED]

To achieve the objectives of this study, finite difference simulations are used to evaluate the stress states and the displacements in the surrounding rock of Gallery No. 2 before and during various gas storage cycles. In these cycles, the gas pressure is varied between the proposed

minimum and maximum operating pressures to determine a pressure range that satisfies the four criteria listed at the beginning of this section. The proposed minimum and maximum wellhead pressures for Gallery No. 2 are [REDACTED], respectively.

The in situ stress state is an important input quantity in a geomechanical analysis. In the 1996 study of Gallery No. 1, a literature review was performed to assess the magnitude and range in measured in situ stresses in western New York. The in situ stresses selected for input to the models in the assessment of Gallery No. 1 were based on the highest horizontal stress to vertical stress ratio [REDACTED] measured in western New York [Osnes and Eyermann, 1996]. The in situ stresses used in the study of Gallery No. 1 will be adopted for the geomechanical evaluation of Gallery No. 2. This assumed in situ stress state adds an additional conservative element to this study because [REDACTED]
[REDACTED]

Three-dimensional representations of Gallery No. 1 and Gallery No. 2 are simulated in the finite difference model. The major advantages of using a three-dimensional model versus a two-dimensional model are accurate geometrical representation of the caverns and the ability to model the in situ stress anisotropy. The disadvantage of a three-dimensional model relates to run time and computer hardware requirements. However, substantial improvements in computer hardware and software in recent years now allow for three-dimensional simulations of Gallery No. 2 where a solution is reached within reasonable amount of time.

3.2 STRATIGRAPHIC MODEL

Gallery No. 2 is located in the interbedded salt and shale layers in the [REDACTED] of the Syracuse Formation. Core has been recovered through the interval of the Syracuse Formation from most of the wells drilled in the Watkins Glen cavern field since the mid-1950s, including Well No. 27 and Well No. 28. The core logs indicate that the thickness of the Syracuse Formation is [REDACTED] and the elevation of formation top [REDACTED] dipping [REDACTED] to the [REDACTED] [PB-KBE, Inc., 1995].
[REDACTED]
[REDACTED]

[REDACTED] the Watkins Glen cavern field, the stratigraphic details that most affect the stability of Gallery No. 2 are those in the immediate vicinity of the gallery. A 1961 open-hole well log from Well No. 31 [Birdwell, 1961] was interpreted and used as a basis to represent the stratigraphy of the Syracuse Formation in the finite difference model of Gallery No. 2. Figure 3-1 shows the interpreted stratigraphy from the Well No. 31 open-hole logs and the east-west projection of Well No. 30 and Well No. 31 based on sonars. Also included in the figure is the stratigraphy used in the 1996 study of Gallery No. 1 and the projections of the caverns associated with Well No. 27, Well No. 28, and

CONTAINS PRIVILEGED INFORMATION
DO NOT RELEASE

RSI-1300-02-004

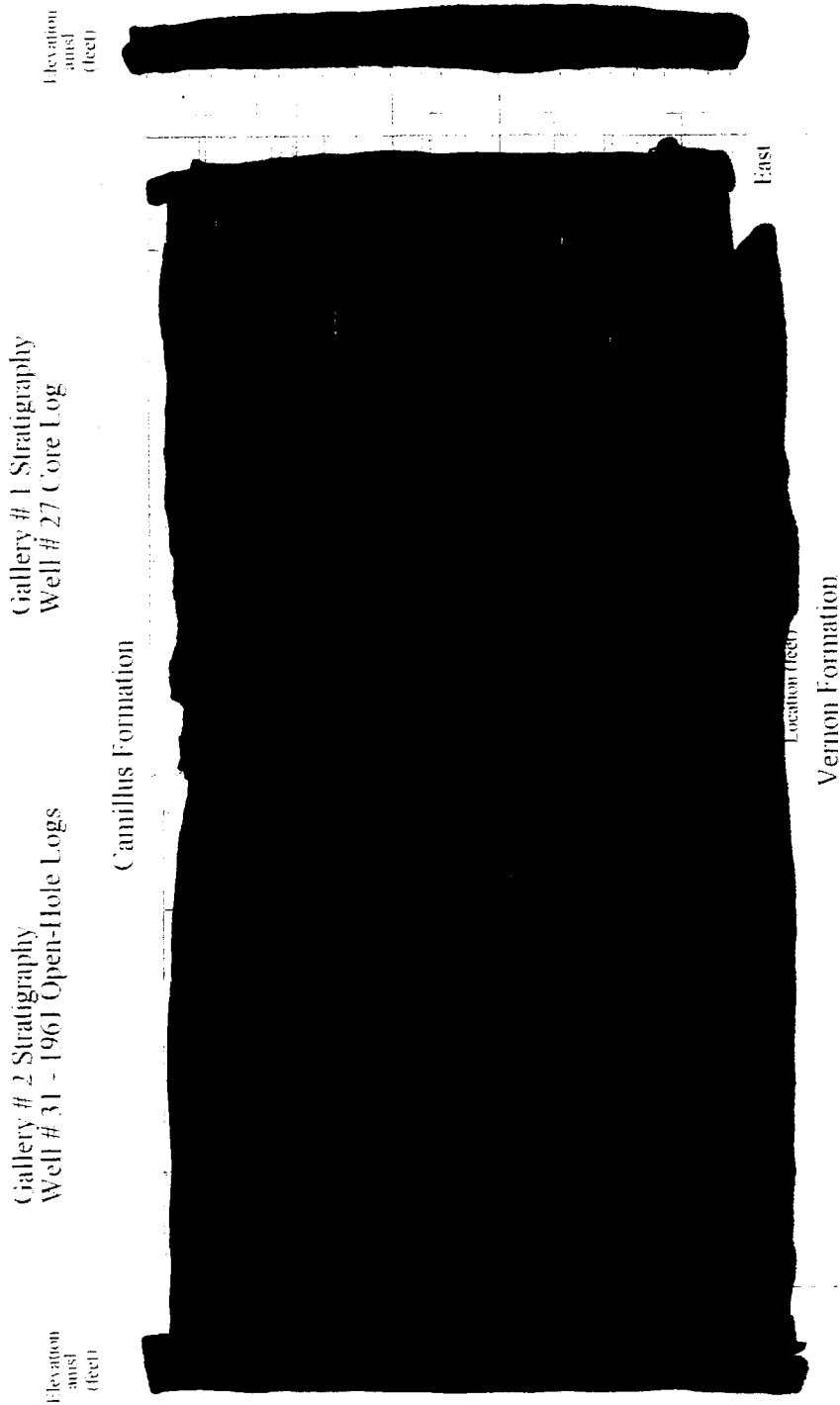


Figure 3-1. Stratigraphy of the Syracuse Formation Based on Core Log From Well No. 27 and Open-Hole Logs From Well No. 31

Well No. 46. The stratigraphy from Well No. 27 has about [REDACTED] than the stratigraphy observed in Well No. 31. The total salt thickness in the Syracuse Formation found from the open-hole logs of Well No. 31 is [REDACTED]. Jacoby [1962] reports a total salt thickness of 378 feet in Well No. 30. The top of the Syracuse Formation in Well No. 31 is located at an elevation of [REDACTED] amsl, which is about [REDACTED] than in Well No. 27. The stratigraphy adapted for the finite difference model is shown in Figure 3-2. Two simplifications were made to the stratigraphy in the Syracuse Formation to limit the model size. [REDACTED] observed in the Well No. 31 stratigraphy were [REDACTED] and the same stratigraphy was used for both Gallery No. 1 and Gallery No. 2. These simplifications should not affect the modeling results for Gallery No. 2 significantly because the [REDACTED]

The stratigraphic column above and below the Syracuse Formation used in the 1996 study of Gallery No. 1 was adopted for this study with one exception. The elevation of the bottom of the Camillus Formation was taken to be equal to the elevation of the top of the Syracuse Formation, based on well logs of Well No. 31. To develop the stratigraphic column above the Syracuse Formation in the 1996 study of Gallery No. 1, the geophysical logs from Well No. 59 were correlated to descriptions of the stratigraphy in other wells at the Watkins Glen cavern field and to general descriptions of the regional stratigraphy [Rickard, 1969; Kreidler et al., 1972; Van Tyne, 1983; Jacobi and Fountain, 1993]. Most of the geologic units above the Syracuse Formation are composed of [REDACTED] although [REDACTED] are predominate in the [REDACTED] the Syracuse Formation. The Vernon Formation, which is composed predominately of [REDACTED] underlies the Syracuse Formation. [REDACTED]

Consequently, the thickness of the Vernon Formation was [REDACTED] based on [REDACTED] [Rickard, 1969; Kreidler et al., 1972].

The complete stratigraphic column modeled in the finite difference simulations is listed in Table 3-1, and the salt and shale layers modeled in the Syracuse Formation are tabulated in Table 3-2. The division into geologic units was based in part on proximity to the gallery with finer divisions near the gallery and assembly of the units into geologic groups farther away. For example, the units below the Vernon Formation were simply defined as "Underlying Groups" because they are so distant from the region of interest around the gallery that their individual thicknesses and properties should not have a significant effect on the simulation results. Nonetheless, when the geophysical logs indicated substantial changes in the properties of adjacent geologic units, the units were divided so that the contrast in the properties could be reflected in the finite difference models [REDACTED]

RSI-1300-02-005

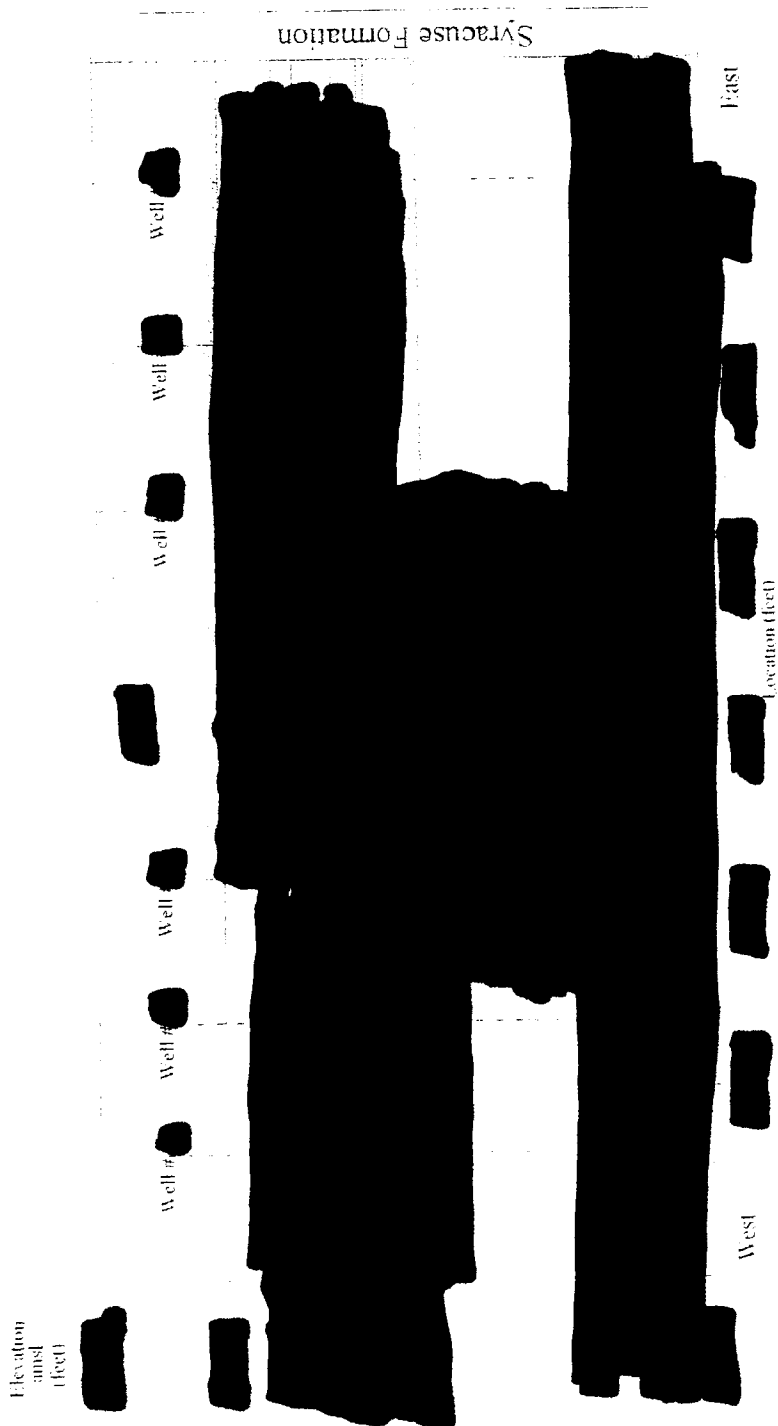


Figure 3-2. Stratigraphy of the Syracuse Formation Used in the Finite Difference Model.

Table 3-1. Stratigraphy Modeled in the Gallery No. 2 Simulations

Geologic Unit	Elevation of Unit Top (ft amsl)	Elevation of Unit Bottom (ft amsl)	Unit Thickness (ft)
Genesee Group	[REDACTED]	[REDACTED]	[REDACTED]
Tully Formation	[REDACTED]	[REDACTED]	[REDACTED]
Hamilton Group	[REDACTED]	[REDACTED]	[REDACTED]
Onondaga Formation	[REDACTED]	[REDACTED]	[REDACTED]
Tristates Group	[REDACTED]	[REDACTED]	[REDACTED]
Helderberg Group	[REDACTED]	[REDACTED]	[REDACTED]
Akron Formation	[REDACTED]	[REDACTED]	[REDACTED]
Bertie Formation	[REDACTED]	[REDACTED]	[REDACTED]
Camillus Formation	[REDACTED]	[REDACTED]	[REDACTED]
Syracuse Formation	[REDACTED]	[REDACTED]	[REDACTED]
Vernon Formation	[REDACTED]	[REDACTED]	[REDACTED]

(a) Ground level at Well No. 31.

Table 3-2. Stratigraphy Within Syracuse Formation Modeled in the Gallery No. 2 Simulations

Geologic Unit	Elevation of Unit Top (ft amsl)	Elevation of Unit Bottom (ft amsl)	Unit Thickness (ft)
Salt	[REDACTED]	[REDACTED]	[REDACTED]
Shale	[REDACTED]	[REDACTED]	[REDACTED]
Salt	[REDACTED]	[REDACTED]	[REDACTED]
Shale	[REDACTED]	[REDACTED]	[REDACTED]
Salt	[REDACTED]	[REDACTED]	[REDACTED]
Shale	[REDACTED]	[REDACTED]	[REDACTED]
Salt	[REDACTED]	[REDACTED]	[REDACTED]
Shale	[REDACTED]	[REDACTED]	[REDACTED]
Salt	[REDACTED]	[REDACTED]	[REDACTED]
Shale	[REDACTED]	[REDACTED]	[REDACTED]

3.3 MATERIAL PROPERTIES

The material properties used to model Gallery No. 2 are taken from the 1996 study of Gallery No. 1 [Osnes and Eyermann, 1996]. A comprehensive investigation of material properties was conducted to represent material behavior accurately in the numerical models of the different geologic units surrounding Gallery No. 1. This section summarizes the material properties from the 1996 study and how they were derived. In addition, material properties specific for the three-dimensional model of Gallery No. 2 are also described.

Of the geologic units listed in Table 3-1, only the Syracuse Formation contains significant thicknesses of salt. The nonsalt units are assumed [REDACTED] and are further assumed [REDACTED]

(This assumption is subsequently checked in the geomechanical analyses by calculating factors of safety against shear failure.) Tensile fracturing of the shale beds in the Syracuse Formation is simulated in the model. The material properties required to simulate the behavior of the nonsalt units are Young's modulus, Poisson's ratio, and density. In addition, the tensile strength for the shale is needed to simulate tensile failure.

Young's modulus and Poisson's ratio are also required to simulate the salt units in the Syracuse Formation that are listed in Table 3-2, but the inelastic response of these units is more important. In the salt beds, viscoplastic (creep) behavior is modeled in addition to the elastic response.

3.3.1 Elastic Properties

The elastic properties of the Camillus Formation that overlie the Syracuse Formation and the salt from the Syracuse Formation were determined by laboratory testing of core recovered from Well No. 58 (salt only) and Well No. 59 [Pfeifle, 1996]. The [REDACTED] from Well No. 59 were taken from [REDACTED] in the depth interval of [REDACTED] feet below the kelly bushing [REDACTED] feet amsl to [REDACTED] feet amsl) and are described as [REDACTED] in the core log [Vogt, 1995]. The salt specimens were taken from the [REDACTED] (cf. Figure 3-1) in the depth interval of [REDACTED] feet [REDACTED] amsl to [REDACTED] amsl).

Young's modulus and Poisson's ratio of the six Camillus Formation specimens varied from [REDACTED] and from [REDACTED] respectively. In the finite difference simulations, a Young's modulus and Poisson's ratio of [REDACTED] psi and [REDACTED] were assigned to the Camillus Formation. These values are equal [REDACTED] A density of [REDACTED] was assigned to the Camillus Formation based on the [REDACTED] of the unit that was indicated in the geophysical logs of Well No. 59.

Four measurements of Young's modulus and Poisson's ratio were made in the laboratory testing of the salt specimens. The average values of these properties were [REDACTED] psi and [REDACTED] respectively, with standard deviations of [REDACTED] and [REDACTED]. The average values were used for the elastic properties of all of the salt beds in the Syracuse Formation. A density of [REDACTED] was assigned to the salt beds based on the average density indicated in the portion of the geophysical logs of Well No. 59 in the upper salt of the Syracuse Formation.

The elastic properties of the geologic units above the Camillus Formation were estimated by scaling the dynamic values of Young's modulus and Poisson's ratio determined from the density and sonic velocity logs of Well No. 59. The elastic properties of the shale layers in the Syracuse Formation and of the geologic units below the Syracuse Formation were [REDACTED]. Their elastic properties were [REDACTED]. The Vernon Formation that underlies the Syracuse Formation is [REDACTED] and its elastic properties also were [REDACTED]. In addition, the [REDACTED]

[REDACTED] These units are so distant from the region of interest around Gallery No. 2 that the values of their elastic properties should not have a significant effect on the modeling results. Published values of the elastic properties of rock in and below the Vernon Formation [Carmichael, 1982] indicate these are reasonable assumptions.

Table 3-3 lists the values of the densities and elastic properties specified in each of the geologic units in the stratigraphic model of Gallery No. 2. The thickness for each unit is also included in Table 3-3. The values of Young's modulus in the [REDACTED] [REDACTED] than the values in most of the geologic units, as expected because these units are composed predominately of [REDACTED] which generally are [REDACTED] that compose most of the other geologic units.

3.3.2 Salt Creep Characterization

The deformation rate of salt can be decomposed into thermal expansion, elastic deformation, and inelastic deformation. The inelastic deformation is highly stress-, temperature-, and rate-dependent. It is comprised of both viscoplastic (creep) and brittle components, with the viscoplastic component usually dominating in the ranges of stress and temperature expected in the salt beds in the Syracuse Formation surrounding Gallery No. 2.

Six multistage triaxial compression creep tests were performed on salt recovered from Well No. 58 and Well No. 59 in the 1996 study of Gallery No. 1 [Pfeifle, 1996]. The creep strain data from the tests were used to fit parameters for the Munson-Dawson multimechanism constitutive model. The Munson-Dawson constitutive model was used in the finite element simulations of Gallery No. 1 to model creep behavior of salt. The three-dimensional, finite

For a triaxial compression laboratory test $\dot{\epsilon}_e$ is the axial creep strain and σ_e is the stress difference $(\sigma_1 - \sigma_3)$. The material properties A_1 , A_2 , n_1 , and n_2 were determined from Munson-Dawson parameters using a temperature of [REDACTED] which is the estimated in situ temperature at the top of the Well No. 30 cavern (see Section 3.4.2). Figure 3-3 shows steady-state creep rates versus effective stress for the Munson-Dawson constitutive model and the two-component power law. The parameters for the power law are listed in Table 3-4.

[illegible]

(b) Total thickness of multiple beds.

Figure 3-3. Steady-State Creep Rates for the Munson-Dawson Model and the Two-Component Power Law.

Table 3-4. Creep Parameters for Salt

Parameter for Salt	Units	Value
[REDACTED]	[REDACTED]	[REDACTED]
[REDACTED]	[REDACTED]	[REDACTED]
[REDACTED]	[REDACTED]	[REDACTED]
[REDACTED]	[REDACTED]	[REDACTED]

3.3.3 Salt and Nonsalt Strength

The stress states predicted in the geomechanical model of Gallery No. 2 were examined to determine:

- The potential for salt dilation (microfracturing)
- Shale shear failure
- Salt and shale tensile fracturing.

Stress states causing dilation (microfracturing) of the salt in the gallery's walls or roof can result in spalling at these locations because the accumulated damage can weaken the salt. Stress states causing shear failure in the nonsalt strata above the gallery may result in casing string damage or even cavern collapse; shear failure in the webs surrounding the gallery also can lead to structural instability.

All rock types have very limited tensile strengths. When these tensile strengths are exceeded, tensile fracturing occurs perpendicular to the direction of the least-compressive (most tensile) principal stress, and the opening of these tensile fractures relieves the tensile stresses. Depending on the orientations and locations of the tensile fractures, tensile failure may cause instability of underground openings. Regardless of orientation, tensile fractures can increase the porosity and may increase the ability of fluids to flow through the rock in the areas where tensile fracturing occurs. Consequently, the least-compressive principal stresses predicted in the salt and nonsalt strata surrounding and overlying the gallery were compared to the respective tensile strengths of the salt and nonsalt to assess the extent of any tensile fracturing.

Each of these strength criteria are described separately in the following sections.

3.3.3.1 Salt Dilation Criterion

The viscoplastic deformation of salt is isovolumetric, which means that the volume of the salt remains constant during creep deformation. An increase in salt volume, a phenomenon referred to as dilation, indicates the formation of microfractures within the salt. A criterion used to determine whether or not a stress state is one that results in salt dilation has been previously developed based on laboratory testing of Avery Island Dome salt and Waste Isolation Pilot Plant (WIPP) bedded salt [Ratigan et al., 1991]. Two stress measures are used in defining the dilation criterion: the first invariant of the stress tensor (I_1) and the second invariant of the deviatoric stress tensor (J_2). These two stress measures are defined as follows:

$$I_1 = \sigma_1 + \sigma_2 + \sigma_3 \quad (3-2)$$

$$J_2 = \frac{1}{6} \left[(\sigma_1 - \sigma_2)^2 + (\sigma_2 - \sigma_3)^2 + (\sigma_3 - \sigma_1)^2 \right] \quad (3-3)$$

where:

$\sigma_1, \sigma_2, \sigma_3$ = principal stress components.

Ratigan et al. [1991] concluded that stress states satisfying the following inequality generally did not result in dilation of salt test specimens:

$$\sqrt{J_2} \leq 0.27 I_1 \quad (3-4)$$

In the creep testing of the salt from Well No. 58 and Well No. 59 [Pfeifle, 1996], the axial stress (σ_1) and the confining pressure (σ_2 and σ_3) were controlled such that $\sqrt{J_2}$ remained constant in all stages of each test while I_1 was incrementally decreased in each stage [Pfeifle, 1996]. The volumetric strains were calculated from the axial and radial strains measured in the creep tests. The magnitude of the volumetric strain began to increase in the last stages of some of the tests, indicating a stress state that causes dilation of the Syracuse salt.

Five constant mean stress (CMS) tests were also performed on salt core from Well No. 58 (three tests) and Well No. 59 (two tests) [Pfeifle, 1996]. The CMS tests are quasi-static triaxial compression tests with much shorter durations than creep tests. In a CMS test, the specimen is initially loaded hydrostatically (axial stress equals confining pressure). Then the axial stress and confining pressure are continually changed in such a way that the mean stress, which is directly proportional to I_1 , remains constant. As the axial stress increases and the confining pressure decreases, the value of $\sqrt{J_2}$ increases. The onset of dilation corresponds to the stress state at which the volumetric strain begins to increase.

The stress state in each stage of the creep tests on Syracuse Formation salt is plotted as either a dilating or nondilating stage in Figure 3-4. The stress states at which the onset of

Figure 3-4. Dilation Response of Salt From Well No. 58 and Well No. 59 Based on Creep and Constant Mean Stress Tests [Pfeifle, 1996].

dilation was observed in the CMS tests also are plotted in this figure. In addition, the dividing line between dilating and nondilating stress states that was recommended by Ratigan et al. [1991] for Avery Island and WIPP salt (Equation 3-4) is plotted in Figure 3-4. The Syracuse salt from Well No. 58 and Well No. 59 appears to exhibit a dilation limit [REDACTED] that is based on substantially more data. [REDACTED]

This evaluation of salt dilation is made in terms of the "damage potential" (DP) which indicates the proximity of a stress state to the dilation limit. The damage potential is defined as follows:

$$DP = \frac{\sqrt{J_2}}{I_1} \quad (3-5)$$

The likelihood of salt dilation increases as the value of DP increases, and according to Equations 3-4 and 3-5, the salt will dilate if the value of DP is greater than 0.27.

3.3.3.2 Shear Failure Criterion for Nonsalt Strata

The criterion used to determine whether or not a stress state is one that results in shear failure of the nonsalt strata is based on laboratory testing of [REDACTED] core from Well No. 59 [Pfeifle, 1996]. Six constant strain rate tests were performed. In these tests, the confining pressure is held constant at [REDACTED] psi while an axial strain rate of [REDACTED] is imposed until the specimen fails. The stress measures used in defining the failure criteria are the same as those used in the dilation criteria for salt: the first invariant of the stress tensor, I_1 , and the square root of the second invariant of the deviatoric stress tensor, $\sqrt{J_2}$.

A failure limit has been established in stress space based on failures measured in laboratory triaxial compression tests. Plotted in Figure 3-5 are the stress states in the tested specimens at the time of failure. The failure limit developed from these tests (also shown in Figure 3-5) was determined by a least-squares fit to the failure stress states. The failure limit for the specimens from the [REDACTED] can be expressed mathematically in terms of the stress invariants (given in psi) as:

[REDACTED] (3-6)

Factors of safety are used to quantify the potential for shear failure in the nonsalt strata. The factor of safety is defined as the material strength divided by the material stress, which may be written as:

$J_2^{1/2}$ (psi)

RS-1415-8



$$FS = \frac{0.449I_1 + 766}{\sqrt{J_2}} \quad (3-7)$$

where the stress invariants are given in psi. A factor of safety of 1.0 is the limit stress state for shear failure to occur. The likelihood of failure increases with decreasing factor-of-safety values. It is obviously desirable to have a factor of safety greater than the limiting state (i.e., $FS > 1$) to account for geologic uncertainties, such as fractures, that are not present in the specimens tested in the laboratory.

3.3.3.3 Tensile Strength

Geologic materials are much stronger in compression than in tension. The unconfined compressive strength of most rocks is generally about ten times greater than the tensile strength. Therefore, tensile stresses in rocks surrounding natural gas storage caverns should be avoided whenever possible through appropriate design of the underground opening or through specification of the operating pressures.

The tensile strength of rock can be highly variable in addition to being small. Therefore, it is difficult to assign a precise value to the tensile strength of most rocks. The presence of tensile stresses in a geomechanical model indicates the need to address the possibility of tensile fracturing even if the rock exhibits a laboratory tensile strength of several hundred psi.

Laboratory testing of salt core from Wells No. 58 and No. 59 indicates that the tensile strength of the bedded salts in this region is [REDACTED]. The average tensile strength of the salt is [REDACTED] for the core from Wells No. 58 and No. 59, respectively [Pfeifle, 1996]. Laboratory testing of [REDACTED] core from Well No. 59 indicates that the tensile strength of this geologic unit, which [REDACTED] Gallery No. 1 and Gallery No. 2, is variable with an average value of [REDACTED] [Pfeifle, 1996] and ranges from [REDACTED] psi.

In this geomechanical analysis, the shale in the Syracuse Formation is assumed to have a tensile strength of [REDACTED]. The material model used in the geomechanical analysis will [REDACTED] i.e., [REDACTED]

[REDACTED] In addition, the two-component power law assigned to the salt units will not fail the material in tension. Postprocessing of the results determines whether or not tensile stresses and fracturing have occurred.

Tensile fractures can result in pathways for fluid (brine or gas) transport if the fractures become interconnected. It is also important to recognize that the permeability of tensile-stress-induced fractures is a strong function of the pressures acting on the exterior and interior of the fracture.

3.4 IN SITU CONDITIONS

The integrity of the walls and roof of a storage cavern is directly related to the deviatoric stress state resulting from the in situ stress and the stresses exerted on the cavern walls by the fluid in the cavern. Therefore, it is important to model in situ stresses which are representative of those in the vicinity of the storage cavern. Accurate representation of the in situ temperatures is also important because the creep rate of the salt, and thus the closure of the cavern, is dependent upon both stress and temperature.

3.4.1 In Situ Stress Distribution

Principal in situ stresses are generally assumed to be aligned with a coordinate system that is vertical and horizontal. The magnitude of the vertical principal stress is typically assumed to be equal to the weight of the overburden. This assumption was made in the geomechanical analysis of Gallery No. 2 using the densities and thicknesses that are listed in Table 3-3 for the geologic units in the stratigraphic model. In some locations, the differences in the magnitudes of the principal stresses are relatively low. For example, the in situ principal stresses in a salt dome are typically assumed to be equal. However, in most nonsalt locations in North America, the magnitudes of the principal stresses are not equal. The inequality of the principal stresses in most regions is reflected in the regional faulting. The faulting in western New York State suggests that the in situ stresses are not equal in magnitude in the nonsalt strata.

A literature review performed in the 1996 study of Gallery No. 1 revealed that the in situ stress state in western New York State is one in which the principal stress components are not equal [Osnes and Eyermann, 1996]. The two principal horizontal stresses are different from the vertical stress and are also different from each other. Based on regional stress measurements, it appears likely that the minimum horizontal stress at the Watkins Glen site is [REDACTED]. Based on the same regional measurements, the [REDACTED].

The in situ stress state used in the 1996 modeling of Gallery No. 1 will be adopted for this study. The values for the in situ stress are conservative estimates and will result in conservative stresses obtained from the three-dimensional model of Gallery No. 2. The maximum horizontal stress is oriented about [REDACTED]. Consequently, the maximum horizontal stress is assumed to be [REDACTED].

3.4.2 Geothermal Temperature Profile

An in situ temperature borehole log is not available for the Watkins Glen site. The following linear temperature profile was assumed for the analysis based on Hodge et al. [1982]:

$$T = 58 - 0.0143z \quad (3-8)$$

where T is the temperature in degrees Fahrenheit and z is the elevation (amsl) in feet.

The two-component power law used to model salt creep is an isothermal constitutive model. The temperature dependence is included in the leading coefficients A_1 and A_2 . A temperature of [REDACTED] was used when the leading coefficients were derived from the Munson-Dawson parameters used in the 1996 study of Gallery No. 1. A temperature of [REDACTED] corresponds to an elevation of [REDACTED] amsl, which is the approximate location of the [REDACTED].

The circulation of brine during filling of Gallery No. 2 with natural gas and the subsequent natural gas movements will perturb the ambient temperature distribution in the immediate vicinity of the cavern. These perturbations were assumed to have negligible effects on the mechanical behavior of the salt in the vicinity of the gallery and were not modeled.

3.5 PROPERTIES OF CAVERN FLUIDS

The mechanical response of a cavern depends not only on the material properties of the salt and nonsalt surrounding the cavern but also on the material properties of the fluids inside the cavern. Gallery No. 2 is assumed to be filled with saturated brine before being dewatered. During dewatering, the gallery is filled with natural gas. In the simulations, these fluids are represented by equivalent pressures applied as tractions normal to the surfaces of the cavern walls. The fluids are assumed to be essentially stagnant, so at a given depth, the vertical pressure gradient is computed from the fluid's density at that depth. In the following two subsections, the resultant vertical pressure gradients are presented for natural gas and saturated brine.

3.5.1 Natural Gas Properties

The gas pressure, P , in a cavern can be described as:

$$P = P_0 + \int_0^z \rho g dz \quad (3-9)$$

where:

P_0 = wellhead pressure

ρ = density of the gas

g = gravitational acceleration

z = depth below wellhead.

The density of natural gas is dependent on pressure and temperature, both of which change with depth. A compressibility equation for natural gas described by Coker [1993] was used to calculate the density as a function of pressure and temperature. Equation 3-9 was integrated

numerically to determine the pressure-versus-depth data, which can be approximated by a linear pressure gradient in the gas at the various pressures considered in this study.

3.5.2 Brine Properties

Because of the very small compressibility of brine (approximately $1.9 \times 10^{-6}/\text{psi}$), the increase in brine density associated with the hydrostatic pressure increase over the height of Gallery No. 2 is negligible (about 0.1 percent change per 1,000 feet). Consequently, the brine density was assumed to be constant at [REDACTED] resulting in a vertical pressure gradient of [REDACTED]

3.6 NUMERICAL MODELING

The finite difference program, **FLAC^{3D}** [Itasca Consulting Group, Inc., 1997], was used to model the mechanical behavior of the salt and nonsalt strata surrounding Gallery No. 2. This specialized computer program and the finite difference model used to represent Gallery No. 2 are described in the following subsections. The computer program, **SALT SUBSID** [Nieland, 1991], used to estimate the subsidence associated with natural gas storage operations in Gallery No. 2 also is described.

3.6.1 Finite Difference Program

Numerical modeling has proven to be a valuable tool in predictive and comparative analyses of solution-mined caverns. The finite difference program used in the numerical analyses was **FLAC^{3D}**, Version 2.00-109, a three-dimensional explicit finite difference code developed by Itasca Consulting Group, Inc. [1997]. **FLAC^{3D}** is designed to simulate the behavior of structures built of soil, rock, or other materials that may undergo plastic deformation when their yield limit is reached. Materials are represented by polyhedral elements that form a three-dimensional grid, which can be adjusted to fit the shape of the object being modeled. Each element behaves according to a prescribed linear or nonlinear stress-strain law (constitutive model) in response to the applied forces or boundary restraints. If the stresses (or stress gradients) are high enough to cause the material to yield and flow, the grid can actually deform and move with the material represented in the model. **FLAC^{3D}** is based on a "Lagrangian" calculation scheme that is well suited for modeling large distortions.

Because **FLAC^{3D}** was developed primarily for geotechnical applications, it embodies special features to represent accurately the mechanical behavior of geologic materials. **FLAC^{3D}** has six built-in material models ranging from the "null" model, which represents holes (excavations) in the grid, to the shear- and volumetric-yielding models, which include strain hardening/softening behavior, nonlinear shear failure, and compaction. Furthermore, **FLAC^{3D}** has several built-in constitutive models that permit the simulation of highly nonlinear materials (e.g., salt).

The features and capabilities of **FLAC^{3D}** that were required specifically for the simulations of Gallery No. 2 include:

- Kinematic and traction boundary conditions
- Two-component power law constitutive model for viscoplastic behavior of salt
- Capability to simulate in situ stress anisotropy
- Capability to simulate excavation operations
- Capability to simulate materials with limited tensile strengths.

3.6.2 Finite Difference Model

A finite difference model is a numerical model constructed to include the geologic stratigraphy in the immediate vicinity of the natural gas storage cavern and the geometry of the natural gas storage cavern. The boundaries of the finite difference model are selected to approximate the "infinite" extent in a certain direction or are selected to include the important boundaries in the vicinity of the cavern (for example, adjacent caverns).

A three-dimensional finite difference model of solution-mined caverns can accurately represent the cavern configurations if information about cavern geometries is available. The Well No. 30 cavern was last surveyed by sonar in December 1997, and the latest available sonar for Well No. 31 dates back to July 1978. The sonars show [REDACTED]

[Medley, 1993]. Only the [REDACTED]
The remainder of the [REDACTED]

The geometry of the caverns used to define Gallery No. 2 in the model was based on the latest available sonars; hence, the [REDACTED]

[REDACTED] The roofs and the cavern sections extending down to the location of maximum cavern diameters seen in the sonars were accurately replicated in the model. Extending the [REDACTED]

[REDACTED] The maximum diameter for Well No. 30 is the maximum diameter found in the sonar. The maximum diameter used for Well No. 31 is the largest outline of the eight points, which defines the maximum radius from the sonar mirrored in a plan view around the wellbore. This is illustrated in Figure 3-6, which shows a plan view of the Watkins Glen cavern field, the areal extent of the **FLAC^{3D}** model, the maximum cavern radii from sonars, and the maximum cavern radii used in the model.

The boundaries of the model are selected to approximate the adjacent caverns or are selected to approximate an infinite extent. The north and south boundaries were placed approximately halfway between Gallery No. 2 and caverns located north and south of the gallery. The eastern

CONTAINS PRIVILEGED INFORMATION
DO NOT RELEASE

RSI-1300-02-007

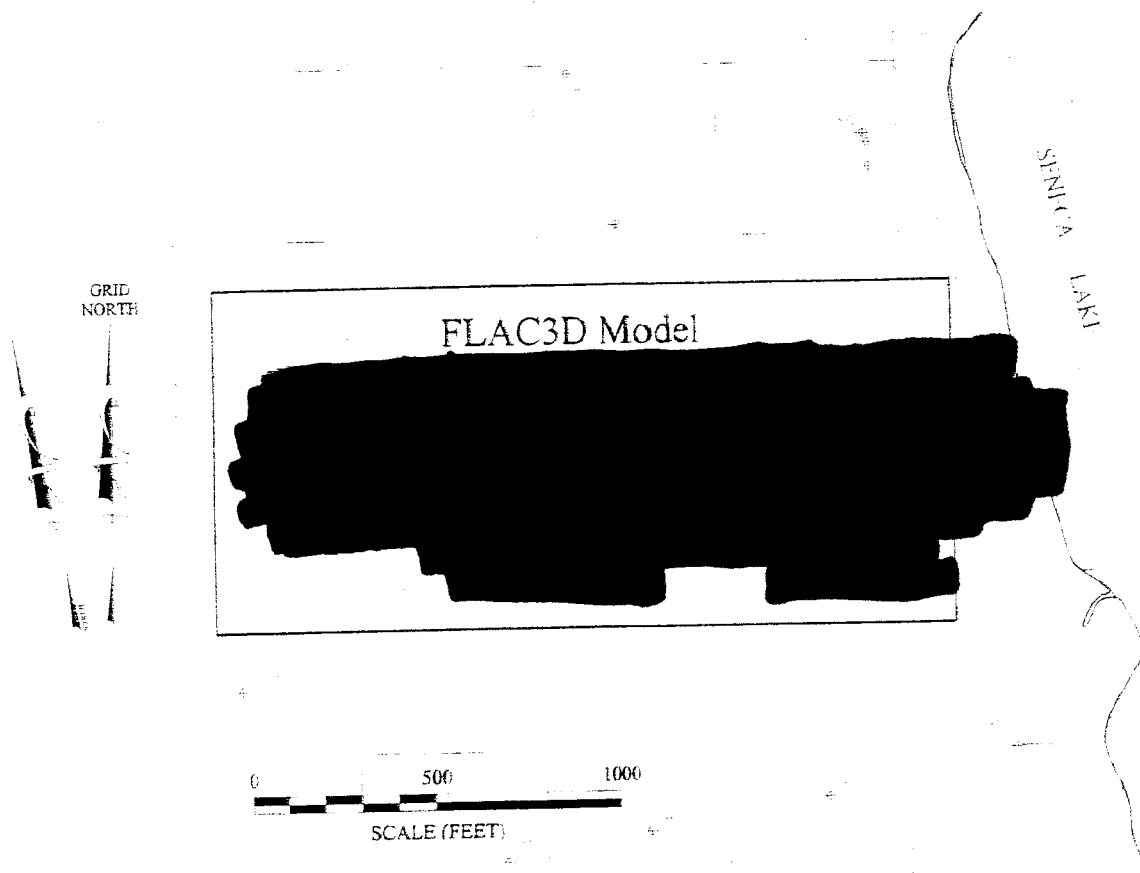


Figure 3-6. Plan View of **FLAC^{3D}** Model and Maximum Radius Outlines.

boundary was truncated in the center of the maximum radius plot for Gallery No. 1, where symmetry about this boundary will represent the whole gallery in the model. To simulate an infinite boundary on the western side of the model, the boundary was truncated as far west as practically possible without exceeding size limitations for the model.

The volumes of the Well No. 30 and Well No. 31 caverns in the model are [REDACTED] respectively. An estimate of the volume of dissolved salt can be obtained from [REDACTED] reported by Medley [1993]. [REDACTED]

The cavern volume based on production records [REDACTED] The equivalent number for Well No. 31 is [REDACTED] This calculation indicates that the caverns in the model are [REDACTED] adds conservatism to the model. The connection between the [REDACTED] is not included in the model because it is believed to have minimal structural impact on the gallery.

[REDACTED] Kinematic boundary conditions imposed on the model reflect the cavern about the west boundary. [REDACTED] The geometry of Gallery No. 1 was obtained from the [REDACTED] as indicated in Figure 3-6. The maximum radius for Gallery No. 1 was taken from a December 1993 sonar. An [REDACTED] The volume of Gallery No. 1 included in the model [REDACTED]

Figure 3-7 shows an east-west cross section through the stratigraphy and a projection of the caverns modeled in the FLAC^{3D} model. The projection of the wellbores is also included in the figure. The top elevations of the Well No. 30, Well No. 31, and Gallery No. 1 caverns included in the model are [REDACTED] and [REDACTED] feet amsl, respectively. The elevations of the cavern bottoms listed in the same order are [REDACTED] feet amsl.

The three-dimensional finite difference model of Gallery No. 2 and Gallery No. 1 is developed with the assumption that the insoluble rubble in the lower parts of the caverns do not provide any structural support. This assumption contributes to the overall conservative approach used in this study.

Figure 3-8 shows various views of the FLAC^{3D} model. The FLAC^{3D} model contains 558,360 elements. The model extends to [REDACTED] amsl. The bottom of the mesh is at [REDACTED] feet amsl. The east-west and north-south dimension

Figure 3-7. East-West Cross Section Through the Stratigraphy and the Projection of the Caverns Included in the Model.

CONTAINS PRIVILEGED INFORMATION
DO NOT RELEASE

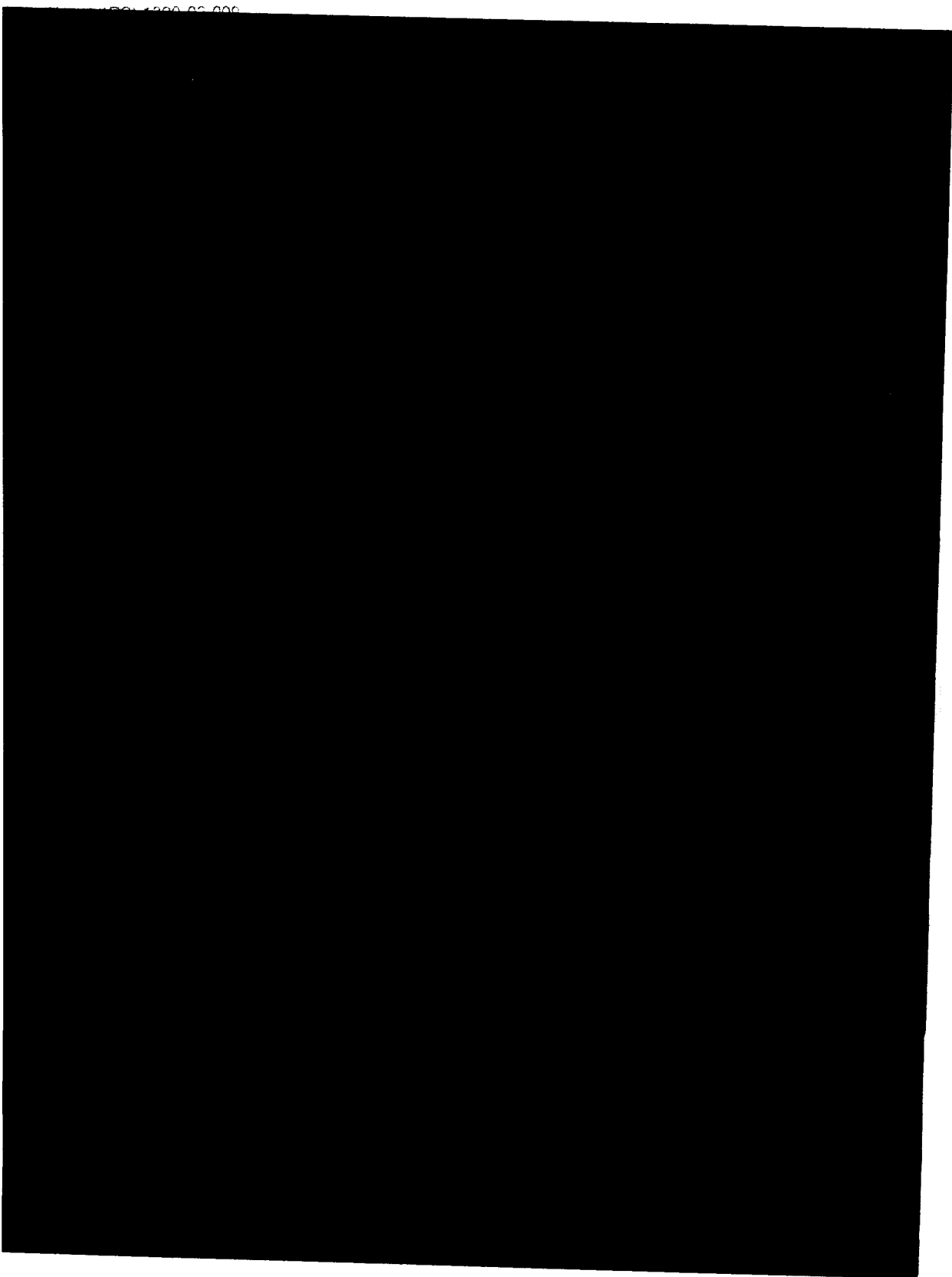


Figure 3-8. Various Views of the FLACsm Model.

of the model are [REDACTED] and [REDACTED] respectively. The four vertical sides of the model are restrained from movement normal to the sides, and the bottom is fixed in the vertical direction. No kinematic boundary conditions are applied to the top of the model, but a vertical traction equal to the weight of the overburden not included in the model is applied at the top of the model.

3.6.3 Subsidence Simulation Program

The ground subsidence resulting from the conversion of Gallery No. 2 to natural gas storage service is calculated using the computer program, **SALT_SUBSID** [Nieland, 1991]. **SALT_SUBSID** is a three-dimensional computer code developed to simulate ground subsidence above solution-mined caverns or dry mines in salt deposits. The code was developed by RESPEC for the Solution Mining Research Institute (SMRI) and is in use by SMRI members throughout the world.

Using **SALT_SUBSID**, the geometry of Gallery No. 2 is approximated as two parallelepipeds with horizontal dimensions of [REDACTED] and a height of [REDACTED] feet for Well No. 30 and [REDACTED] and a height of [REDACTED] feet for Well No. 31. The volumetric closure rate of the gallery during various stages of the natural gas storage cycle is provided to **SALT_SUBSID** as input parameters, and the resulting magnitude and distribution of ground movement is calculated.

Application of **SALT_SUBSID** requires several assumptions, including:

- Rock above the gas storage caverns is homogeneous.
- Rock above the gas storage caverns does not experience any strength failure.
- Interaction of adjacent caverns can be modeled with superposition.

Application of this computer code to numerous bedded and domal salt sites has shown that the predictions of the code are reasonably accurate, despite the assumptions listed above.

4.0 CAVERN OPERATING PRESSURES

The geomechanical behavior of Gallery No. 2 depends directly on the chronology of the operating pressures within the caverns. Although Gallery No. 2 has been used for brine production and LPG storage over its 40-year history, it has been inactive and filled with brine since 1984. During conversion to natural gas storage, Gallery No. 2 will be dewatered by displacing brine with natural gas. During storage service, the gas pressure in the cavern will vary cyclically between the maximum and minimum operating pressures as gas is injected or withdrawn from storage. The amount of time the cavern will experience maximum pressure and the time at minimum pressure will depend to a great degree on market conditions.

The galleries were modeled through [REDACTED] of brine-filled conditions and LPG storage followed by dewatering at maximum cavern pressures, and finally, a series of natural gas storage cycles. In the following sections, the cavern pressures for each of these conditions are presented.

4.1 BRINE AND LPG STORAGE

The stresses in the vicinity of Gallery No. 2 have been significantly altered from the original in situ conditions by the brine production activities and LPG storage operations in the gallery. LPG was stored in the gallery between 1964 and 1984. Because brine was used to displace the LPG, pressure conditions in the cavern during this period are not expected to be significantly different than during brine mining or brine storage. Thus to approximate current conditions in the finite difference model of the caverns, the estimated current geometries of the caverns were assumed to have occurred instantaneously, and pressure distributions equivalent to brine-filled conditions with a wellhead pressure of [REDACTED] were maintained for a [REDACTED] period.

4.2 DEWATERING - CONVERSION TO NATURAL GAS STORAGE

Gallery No. 2 will be dewatered and filled with natural gas by displacing the brine with natural gas. As a cavern is being dewatered, the depth of the gas-brine interface is lowered continuously. The rate at which the gas-brine interface moves downward depends on the dewatering rate and on the cross-sectional area of the cavern at the current location of the gas-brine interface. The elevation of the interface during dewatering of Gallery No. 2 [REDACTED] because the cross-sectional area and porous volume below the [REDACTED]. Thus dewatering of Gallery No. 2 was simulated by [REDACTED]

This method of simulating dewatering is expected to have an effect similar to the actual

dewatering process because the net effect of dewatering is to unload the rock surrounding the gallery. The bulk of this unloading occurs immediately, as soon as the maximum gas pressure is applied to the brine-filled cavern.

[REDACTED]

Documented pressure histories for Gallery No. 1 indicate almost a year at maximum cavern pressure before gas withdrawal and injection started. Thus the maximum pressure condition was maintained for a period of 1 year to approximate the stresses around Gallery No. 2 at the end of dewatering.

4.3 GAS STORAGE

When dewatering is completed in the simulations, Gallery No. 1 and Gallery No. 2 contain natural gas at their maximum gas pressures, [REDACTED] respectively, at their wellheads. The maximum gas pressure for Gallery No. 1 was obtained from the 1996 study of Gallery No. 1 [Osnes and Eyermann, 1996] and corresponds to a pressure of [REDACTED] of depth at the casing seat of Well No. 46. The minimum pressure simulated for both galleries is [REDACTED]. In this analysis, the casing seats for Well No. 31 and Well No. 46 were assumed to be at an elevation of [REDACTED] and [REDACTED] feet amsl, respectively. Table 4-1 lists the simulated wellhead and cavern pressures for Gallery No. 1 and Gallery No. 2 during brine-filled, minimum gas pressure, and maximum gas pressure conditions.

To evaluate the stability of the caverns during gas storage, various gas storage scenarios were examined, including:

- Various combinations of minimum and maximum pressures in Gallery No. 1 and in Gallery No. 2.
- Storage at pressures based on the historical pressure in Gallery No. 1.

Figure 4-1 shows the pressure history for each of the minimum/maximum pressure combinations that were simulated. As seen in the figure, [REDACTED] for each of the simulations and includes [REDACTED] at brine/LPG conditions followed by [REDACTED] of dewatering the cavern at maximum pressure. Following dewatering, the caverns were either held at [REDACTED] or instantaneously dropped to [REDACTED]. At the end of the [REDACTED] time), cavern pressures were either left unchanged or instantaneously changed from minimum

to maximum or from maximum to minimum pressure. The purpose of these simulations was to evaluate the effects of extreme pressure changes in the galleries and the most extreme pressure differentials between the two galleries.

Table 4-1. Cavern Operating Pressures for Gallery No. 1 and Gallery No. 2

Condition	Wellhead Pressure (psi)	Casing Shoe Pressure (psi)	Gas/Brine Pressure Gradient (psi/ft)
<i>Gallery No. 1 (Based on Well No. 46)^(a)</i>			
Brine Filled	██████	██████	██████
Maximum Gas Pressure	██████	██████	██████
Minimum Gas Pressure	██████	██████	██████
<i>Gallery No. 2 (Based on Well No. 31)</i>			
Brine Filled	██████	██████	██████
Maximum Gas Pressure	██████	██████	██████
Minimum Gas Pressure	██████	██████	██████

(a) Values are slightly different than reported in the 1996 study of Gallery No. 1 [Osnes and Eyermann, 1996] because the FLAC^{3D} model used in this study has surface elevation defined at the wellhead of Well No. 31.

Figure 4-2 illustrates the simulated annual pressure cycles for Gallery No. 1 and Gallery No. 2. The gas storage cycle for Gallery No. 1 is an annual pressure cycle developed to approximate the historical monthly pressure records from Gallery No. 1. A similar cycle was developed for Gallery No. 2 by adjusting the Gallery No. 1 cycle to vary between the minimum and maximum allowable gas pressures for Gallery No. 2. These two pressure cycles were implemented simultaneously in the model and repeated ████████ to give a final simulation time of ████████

A gallery interaction study was also performed. Results from two elastic simulations were used to evaluate the interaction between Gallery No. 1 and Gallery No. 2. The gravitational forces and in situ stresses were set to ████████ in these two simulations, and the material models were defined as elastic. These simplifications to the model enable direct insight into how pressurizing Gallery No. 1 affects the stress state around Gallery No. 2 and how the stress state around Gallery No. 1 is affected by pressurizing Gallery No. 2. The maximum pressure change Gallery No. 1 can experience is ████████ which is the difference between the permitted minimum and maximum operating pressures. The difference between the simulated minimum



Figure 4-2. Simulated Annual Pressure Cycles for Gallery No. 1 and Gallery No. 2.

CONTAINS UNCLASSIFIED INFORMATION
DO NOT RELEASE

and maximum pressures in Gallery No. 2 is [REDACTED]. These pressure changes were simulated to evaluate the interaction between the caverns for the largest pressure differentials the galleries are expected to experience. Therefore, in the first simulation, Gallery No. 1 was [REDACTED] while Gallery No. 2 was [REDACTED]. Gallery No. 2 was [REDACTED] in the second simulation while Gallery No. 1 was [REDACTED].

5.0 MODELING RESULTS

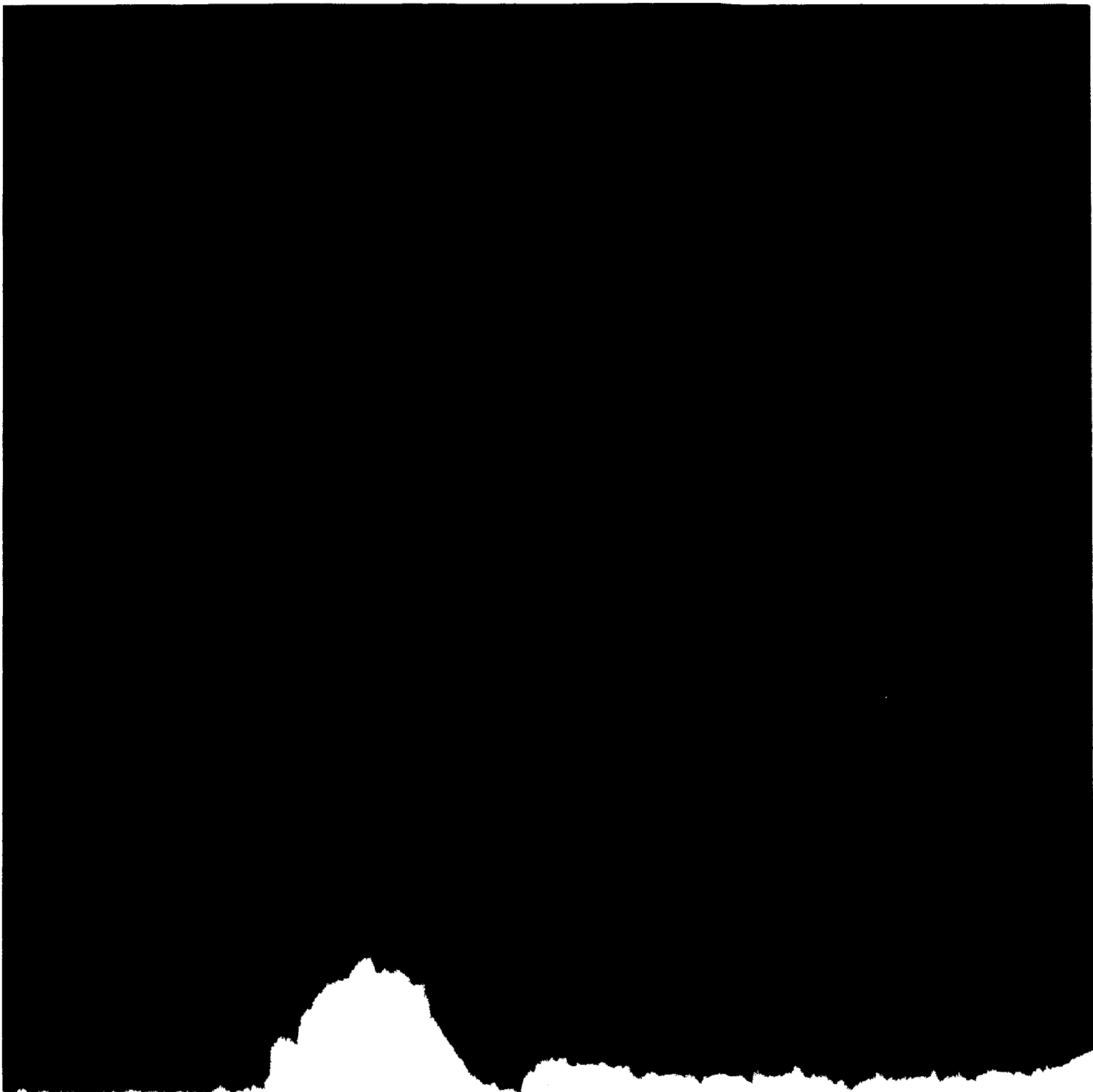
The results of the finite difference simulations of Gallery No. 2 are presented in this chapter. The results are presented in terms of the damage potentials in the salt (Equation 3-5), factors of safety in the nonsalt strata (Equation 3-7), and regions of tensile fractures in both the salt and nonsalt strata. These quantities are used to evaluate the structural stability of the gallery and the potential for interconnection with adjacent caverns. The largest change in principal stress is used to evaluate the interaction between Gallery No. 1 and Gallery No. 2. The rates of cavern closure calculated in the finite difference simulations and the associated surface subsidence are also presented in this chapter.

The interaction between Gallery No. 1 and Gallery No. 2 is an important aspect of this study. If interaction between the galleries is significant, it could inhibit the ability to operate Gallery No. 1 and Gallery No. 2 independently of each other. If the interaction between the galleries is not significant, the stability of Gallery No. 2 will be controlled by the gas pressure in Gallery No. 2 and not be significantly affected by the gas pressure in Gallery No. 1. The results from the simulation of the interaction between the galleries are presented first, in Section 5.1. Sections 5.2 and 5.3 present the results from the brine-filled and dewatering simulations, respectively. The results from simulation of gas storage at minimum pressure are presented in Section 5.4. The predictions of cavern closure and subsidence rates are discussed in Section 5.5.

5.1 INTERACTION BETWEEN GALLERY NO. 1 AND GALLERY NO. 2

The interaction between Gallery No. 1 and Gallery No. 2 was evaluated in terms of the largest change in principal stress around one gallery caused by pressurizing the other gallery. Only Gallery [REDACTED] and only [REDACTED]. The forces applied to the model in these simulations were derived from cavern pressure only, and consequently, any change in the stress state around the [REDACTED] must be caused by the [REDACTED].

The maximum pressure change Gallery No. 1 is expected to experience is [REDACTED] which is the difference between the permitted minimum and maximum operating pressures. Figure 5-1 shows a plot of the maximum change in principal stress at the cavern surfaces of Gallery No. 2 for a [REDACTED] pressure change in Gallery No. 1. A horizontal plane located at an elevation of [REDACTED] feet amsl is also included in the figure to show the stress distribution in plan view. An outline of the cavern perimeter of Gallery No. 1 can be seen in the lower right-hand corner of the figure. Increasing the pressure in Gallery No. 1 by [REDACTED] results in a [REDACTED].



the [REDACTED] The [REDACTED] The simulated pressure is changed instantaneously in the simulation; whereas, in reality, it will take time to inject or withdraw the gas to reduce or increase the gas pressure. Salt creep will tend to reduce stress differences during this time period, and consequently, the stress change predicted in this model is [REDACTED]

The maximum pressure change Gallery No. 2 is expected to experience is [REDACTED] which is the difference between the proposed minimum and maximum operating pressures. A [REDACTED] pressure increase in Gallery No. 2 results in a [REDACTED]

Based on these analyses, the maximum perturbation in the stress field about either gallery caused by [REDACTED] With this [REDACTED]

[REDACTED] the interaction between Gallery No. 1 and Gallery No. 2 is [REDACTED] The web between the galleries is [REDACTED]

[REDACTED] The results for Gallery No. 2 are presented in the next sections. These results will primarily be affected by the gas pressure conditions in Gallery No. 2.

5.2 BRINE AND LPG STORAGE

During the last [REDACTED] Gallery No. 2 has been filled with brine and LPG. This period was modeled to predict the conditions around the gallery as they exist before conversion to natural gas storage. Brine-filled conditions were also modeled for Gallery No. 1 during this time period. The brine pressure maintained at the surfaces of the galleries during the simulation is based on a pressure gradient of [REDACTED] wellhead pressure.

Figure 5-2 shows the salt damage potentials on the surface of Gallery No. 1 and Gallery No. 2 at the end of the [REDACTED] period. The damage potential values in the salt are mostly between [REDACTED] for both galleries, with the exception of [REDACTED] where the values range between [REDACTED] The maximum salt damage potentials are [REDACTED]

The factors of safety predicted in the nonsalt strata in the vicinity of Gallery No. 1 and Gallery No. 2 are shown in Figures 5-3 and 5-4. The figures show an east-west cross section

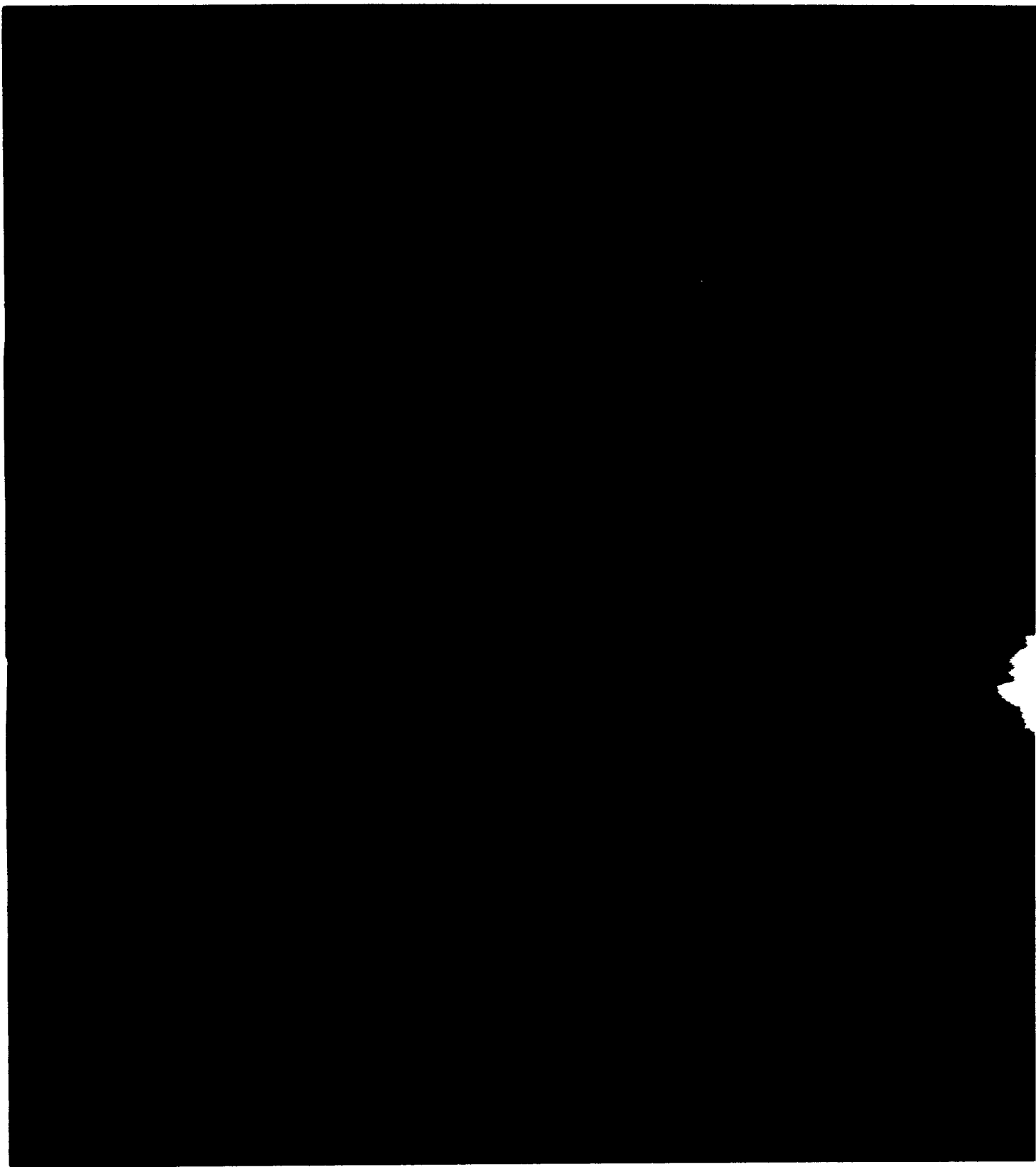


Figure 5-2. Damage Potential Predicted on the Surfaces of Gallery No. 1 and Gallery No. 2 After 40 Years of Brine Production and LPG Storage.



Figure 5-3. Northern View of Factors of Safety Predicted in the Nonsalt Strata Around Gallery No. 1 and Gallery No. 2 After 40 Years of Brine Production and LPG Storage.

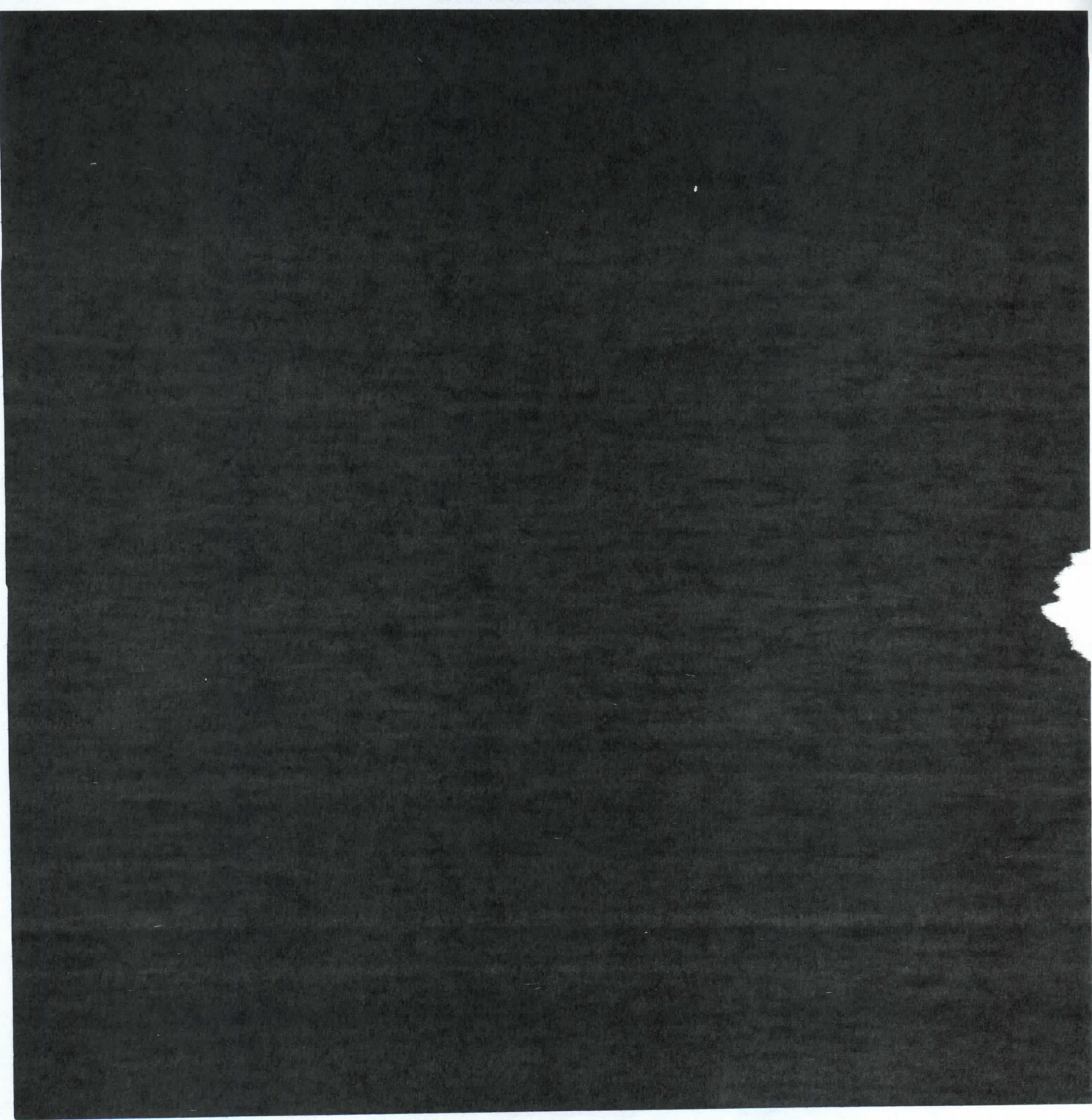


Figure 5-4. Southern View of Factors of Safety Predicted in the Nonsalt Strata Around Gallery No. 1 and Gallery No. 2 After 40 Years of Brine Production and LPG Storage.

cutting through the wellhead location of Well No. 31. In Figure 5-3, the viewing direction is to the north, and in Figure 5-4, the viewing direction is to the south.

The safety factors everywhere in the geologic units overlying Gallery No. 2 are [REDACTED] indicating that the [REDACTED]. The safety factors along the [REDACTED].

Safety factors in the nonsalt units around Gallery No. 1 are predicted to be [REDACTED]. brine storage in the 1996 study [Osnes and Eyermann, 1996]. Figure 5-5 shows the areas that experienced [REDACTED] during the simulation of [REDACTED] of brine production and LPG storage. [REDACTED] is predicted around Gallery No. 2. Comparing the regions of [REDACTED] in Figure 5-5 to the areas with [REDACTED] in Figures 5-3 and 5-4 reveals that the areas with [REDACTED].

Analysis of the principal stresses revealed that the predominate orientation of the [REDACTED]. Therefore, any [REDACTED] will be [REDACTED]. This [REDACTED] does not produce [REDACTED] however, it will [REDACTED] and may possibly [REDACTED]. The regions of [REDACTED] predicted in the brine-filled simulations are limited to [REDACTED]. Consequently, [REDACTED].

It is important to recognize that the [REDACTED] and subsequent [REDACTED] predicted in the finite difference model is a direct result of the assumed strength of the [REDACTED]. Since the [REDACTED] deform differently, either the [REDACTED]. The [REDACTED] in the model; i.e., [REDACTED]. If the [REDACTED] of the [REDACTED] in the model, the extent of the [REDACTED] would be [REDACTED]. However, [REDACTED] would be exhibited.

5.3 DEWATERING - CONVERSION TO NATURAL GAS STORAGE

Dewatering of Gallery No. 2 was simulated at maximum gas pressure. The maximum pressure was maintained for a [REDACTED] period.



When Gallery No. 2 is dewatered by injection of natural gas at the maximum pressure, the pressures applied to the surface of the gallery increase. Consequently, the rock around the gallery is unloaded¹ during dewatering. In turn, the potentials for [REDACTED] and [REDACTED] and the [REDACTED]

This [REDACTED] is clearly reflected in the [REDACTED] at the end of the dewatering period, which is shown in Figure 5-6 (cf. Figure 5-2). The [REDACTED] on the surface of Gallery No. 2 are shown both from the south and from the north in the figure. The [REDACTED] Most of the salt has values [REDACTED] whereas, the majority of the salt at the end of the brine-filled period had [REDACTED]

The [REDACTED] in the nonsalt strata also [REDACTED] as indicated by Figures 5-7 and 5-8. Comparing these figures to Figures 5-3 and 5-4 reveals that the [REDACTED] at the end of the dewatering. The areas with [REDACTED] have [REDACTED] at the wall of [REDACTED] and the areas with [REDACTED] have [REDACTED] Similarly, for the [REDACTED] the [REDACTED] are [REDACTED] after [REDACTED] Also, the conditions in the shale around Gallery No. 1 have [REDACTED] Finally, there is [REDACTED]

5.4 NATURAL GAS STORAGE SCENARIOS

As discussed in the preceding section, increasing the pressure inside Gallery No. 2 from the brine-filled condition to the maximum pressure [REDACTED] Maintaining the pressure inside the gallery at the maximum value for an extended period of time, as done during the dewatering simulation, [REDACTED] Further, restoring the pressure to the maximum value after withdrawal of the gas to the minimum pressure [REDACTED]

All of the gas cycles described in Section 4.3 including the various minimum/maximum pressure combinations and a 5-year natural gas cycle based on the pressure history of Gallery No. 1 were simulated. Results from the various minimum/maximum pressure simulations show that the pressure condition in [REDACTED] This is consistent with the interaction study described in Section 5.1 which also suggested that the [REDACTED]

¹ In this context, unloading [REDACTED] in the rock surrounding the caverns.

Figure 5-6. Damage Potential Predicted in the Salt Around Gallery No. 2 After 1 Year at Maximum Pressure.

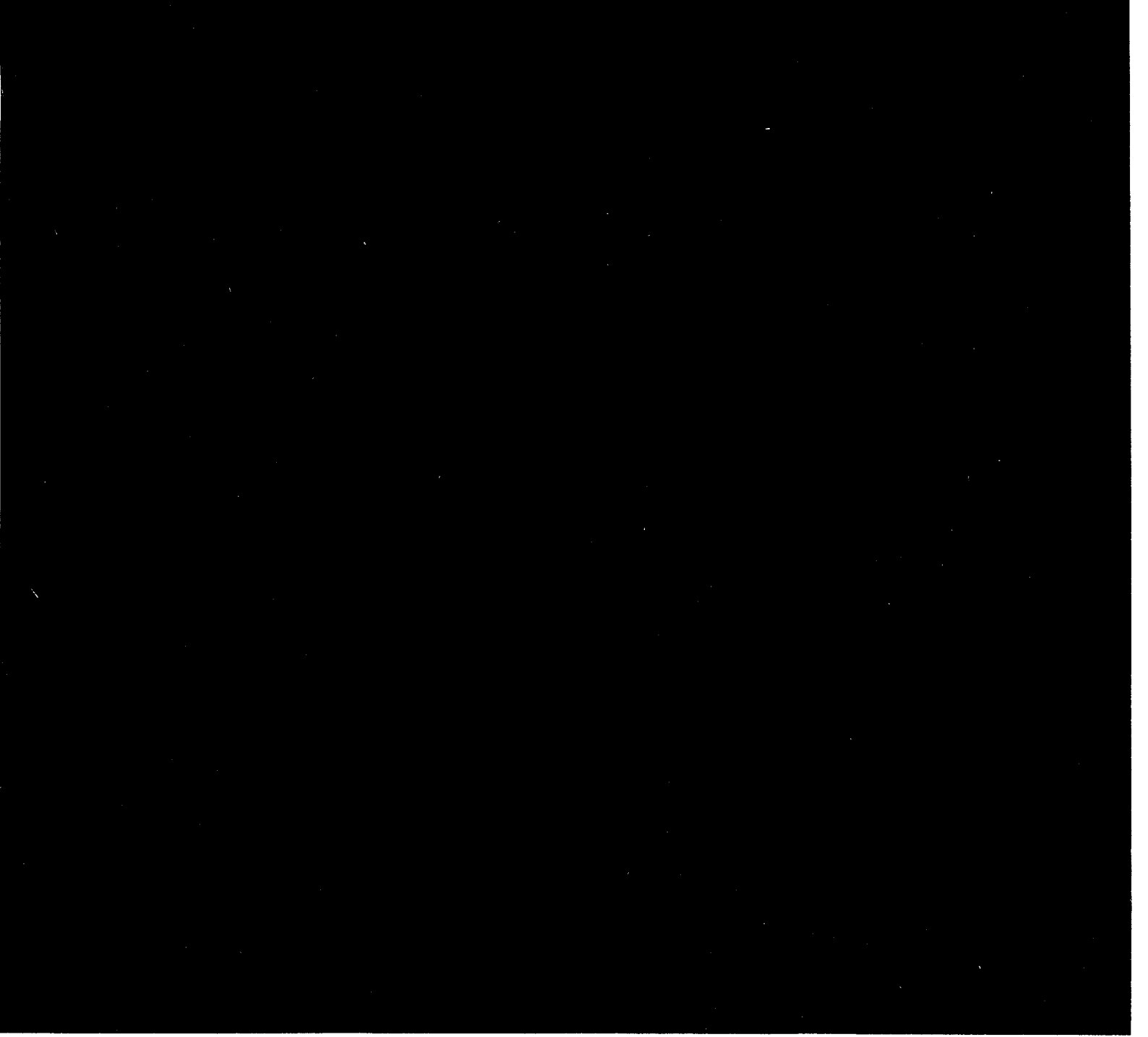


Figure 5-7. Northern View of Factors of Safety Predicted in the Nonsalt Strata Around Gallery No. 1 and Gallery No. 2 After 1 Year at Maximum Pressure.




Figure 5-8. Southern View of Factors of Safety Predicted in the Nonsalt Strata Around Gallery No. 1 and Gallery No. 2 After 1 Year at Maximum Pressure

[REDACTED]
[REDACTED]
[REDACTED] Withdrawal to minimum pressure [REDACTED]
[REDACTED] In turn, the cavern is at the [REDACTED] Although all of the cycles described in Section 4.3 were simulated in this study, only the results for [REDACTED]
[REDACTED]

The [REDACTED] calculated for Gallery No. 2, immediately after [REDACTED] are shown in Figures 5-9 and 5-10, respectively. The [REDACTED] The [REDACTED] is slightly [REDACTED] than at the beginning. This [REDACTED] is expected because [REDACTED]
[REDACTED]

The [REDACTED] calculated in the nonsalt strata are shown in Figures 5-11 through 5-14. Figures 5-11 and 5-12 show the [REDACTED] immediately after reducing the cavern pressure to minimum gas pressure. Figures 5-13 and 5-14 show the [REDACTED] at the end of the 1-year period at minimum gas pressure. Comparing Figures 5-11 and 5-12 to Figures 5-13 and 5-14, respectively, indicates that the [REDACTED] It should be mentioned that [REDACTED] This [REDACTED] is caused by [REDACTED] As the [REDACTED] it [REDACTED] resulting in [REDACTED] The [REDACTED] in the [REDACTED] The [REDACTED] in the [REDACTED] are [REDACTED] Again, the [REDACTED] in this area are caused by [REDACTED] which [REDACTED] The figures also show that the conditions around Gallery No. 2 are generally [REDACTED] Gallery No. 1. The results from the simulations show that the [REDACTED]
[REDACTED]

Figure 5-15 shows the [REDACTED] predicted immediately after lowering the gas pressure to the minimum pressure in Gallery No. 1 and Gallery No. 2. Figure 5-16 shows [REDACTED] minimum gas pressure. The [REDACTED] are [REDACTED] However, the extent of the [REDACTED] limited to [REDACTED] Comparing the [REDACTED] to the [REDACTED] Figures 5-11 through 5-14 clearly reveals the correspondence between the [REDACTED]
[REDACTED]

Figure 5-9. [REDACTED] Around Gallery No. 2 Immediately After
Pressure Reduction to Minimum Pressure

Figure 5-10. [REDACTED] Around Gallery No. 2 After 1 Year at
Minimum Pressure

Geomechanics
RESPEC

Figure 5-11. Northern View of [REDACTED] Predicted in the [REDACTED] Around Gallery No. 1 and Gallery No. 2 Immediately After Pressure Reduction to Minimum Pressure




Figure 5-12. Southern View of [REDACTED] Predicted in the [REDACTED] Around
Gallery No. 1 and Gallery No. 2 Immediately After Pressure Reduction to
Minimum Pressure.




Figure 5-13. Northern View of [REDACTED] Predicted in the [REDACTED] Around
Gallery No. 1 and Gallery No. 2 After 1 Year at Minimum Pressure

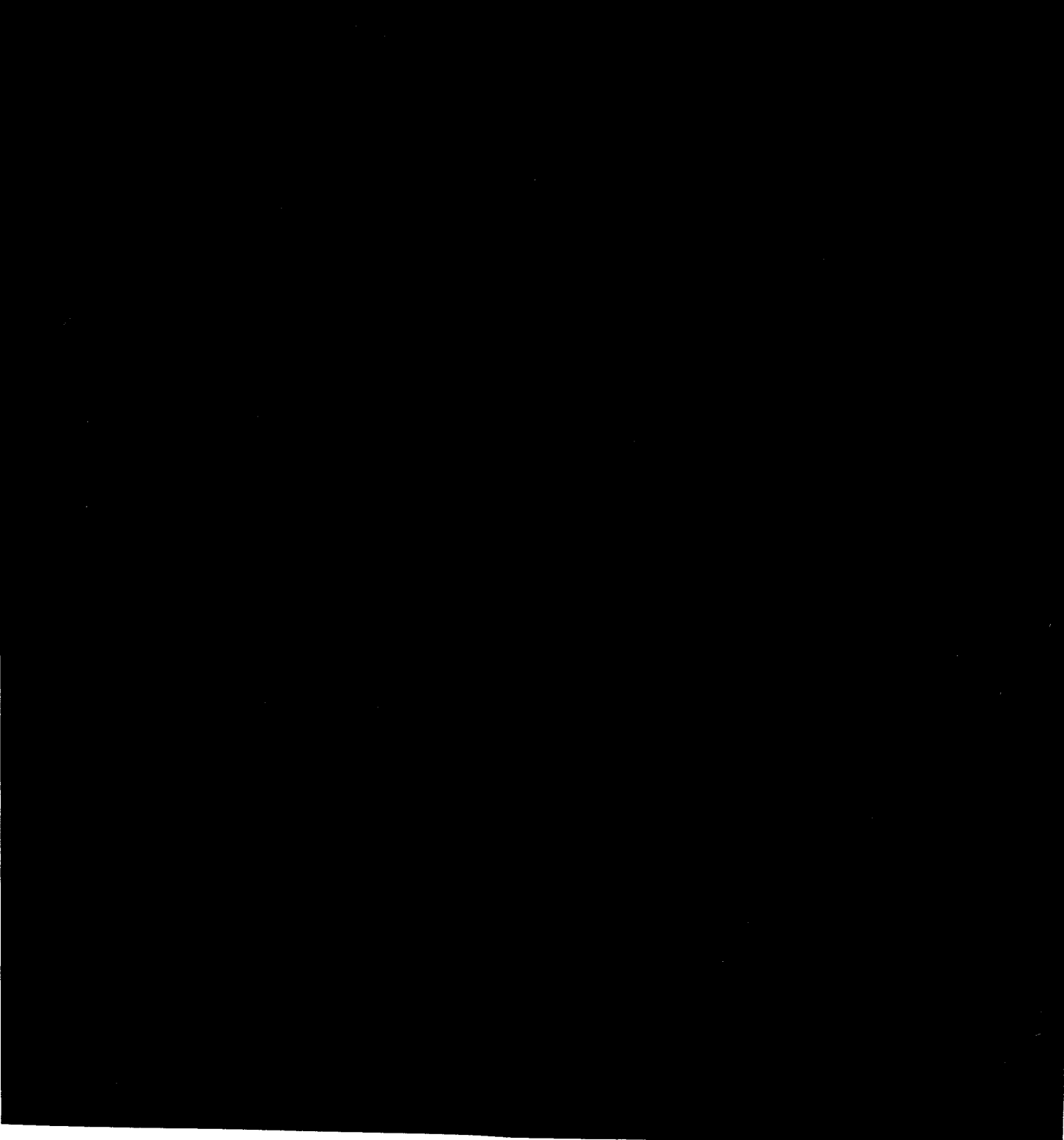


Figure 5-14. Southern View of [REDACTED] Predicted in the [REDACTED] Around
Gallery No. 1 and Gallery No. 2 After 1 Year at Minimum Pressure.

Figure 5-15. [REDACTED] Predicted Immediately After Reducing Pressures
in Gallery No. 1 and Gallery No. 2 to Minimum Pressure.

Figure 5-16. [REDACTED] Predicted After 1 Year at Minimum Pressure for
Galiery No. 1 and Galiery No. 2.

CONTAINED UNCLASSIFIED INFORMATION
DO NOT RELEASE

Again, [REDACTED] is a direct result of the [REDACTED] of the [REDACTED]. If the [REDACTED] of the [REDACTED] in the models, the [REDACTED]. However, the [REDACTED] In the model, the [REDACTED] layer. Thus the [REDACTED]. Using [REDACTED] for estimating [REDACTED] because it predicts [REDACTED] than if [REDACTED] conditions were assigned to the interfaces.

[REDACTED] are not predicted in the [REDACTED]. In addition, no [REDACTED] are predicted in the [REDACTED]. Consequently, [REDACTED] is not a concern in the [REDACTED].

The regions of predicted [REDACTED] are limited even after [REDACTED]. Larger areas of [REDACTED] were [REDACTED] in the 1996 study [Osnes and Eyermann, 1996] than the [REDACTED] predicted around [REDACTED] in this study. Further, the model does not predict a continuous region of [REDACTED]. In fact, most of the [REDACTED] are expanding in the [REDACTED] and not in the [REDACTED] toward [REDACTED]. One can state with a high degree of certainty that [REDACTED]. The [REDACTED] is not [REDACTED].

5.5 CAVERN CLOSURE AND SUBSIDENCE RATES DURING GAS STORAGE

Volumetric closure was calculated for Well No. 30, Well No. 31, and Gallery No. 1 for the annual gas storage cycle shown in Figure 4-3. The annual gas storage cycle was simulated as a continuation of the dewatering and gas storage at maximum pressure simulation [REDACTED] and repeated [REDACTED] to yield a final simulation time of [REDACTED]. The volumes of the excavated caverns are evaluated directly in the finite difference model. The volumetric closure is calculated as the change in volume with respect to the initial volume.

Figure 5-17 shows the volumetric closure versus time for the three caverns included in the model. Most of the [REDACTED] shown in the figure is an [REDACTED]. The annual closure rate calculated for the [REDACTED] is about [REDACTED] for Gallery No. 2 and [REDACTED] for Gallery No. 1. The calculated closures are [REDACTED]. The simulations indicate that there will be [REDACTED].



Figure 5-17. Volumetric Closure During [REDACTED]

CONTAINED INFORMATION
NOT RELEASE

The model is [REDACTED] since the [REDACTED] in the finite difference model is [REDACTED]. The salt would be [REDACTED] the cavern, resulting in [REDACTED]. The closure is expected to be [REDACTED] even if the [REDACTED] in the model were [REDACTED].

The annual subsidence rate associated with the closure of Gallery No. 2 after conversion to natural gas storage were calculated using the subsidence modeling program SALT_SUBSID [Nieland, 1991]. The volumetric closure rates from the 5-year gas storage cycle for Well No. 30 and Well No. 31 were used as input to the subsidence program. The estimated increase in the annual subsidence rate is [REDACTED] at the wellhead at both Well No. 30 and Well No. 31. Consequently, cavern closure and subsidence rates have [REDACTED].

6.0 SUMMARY

The operation of Gallery No. 2 in gas storage service over the range of pressures, bounded by a minimum pressure of [REDACTED] and a maximum pressure of [REDACTED] was evaluated using three-dimensional finite difference model simulations. The model includes the [REDACTED] associated with [REDACTED] and a [REDACTED]

[REDACTED] Conservatism was intentionally built into the finite difference model used for geomechanical evaluation of the gas storage in Gallery No. 2. Many of the model input quantities were selected specifically to be consistent with the conservative geomechanical evaluation approach used in the 1996 study of Gallery No. 1 [Osnes and Eyermann, 1996]. The conservatism built into the model includes:

- [REDACTED]
- [REDACTED]
- [REDACTED]
- [REDACTED]
- [REDACTED]
- [REDACTED] ed.

The impact of converting Gallery No. 2 from its current brine-filled condition to gas storage service on surrounding caverns and surface conditions was evaluated. Finite difference simulations predicted that Gallery No. 2 is [REDACTED]

[REDACTED] This conclusion is based on the [REDACTED]
[REDACTED] The surface subsidence caused by gas storage in Gallery No. 2 is [REDACTED]

The structural stability of Gallery No. 2 was assessed by examination of the finite difference modeling results. The modeling results were evaluated based on strength, creep, and dilation properties of the gallery's host formation. The stability evaluation included an assessment of the roof stability of the gallery and the potential for rock spalling from the sidewalls. These assessments are briefly summarized below.

The minimum factor of safety in the nonsalt roof rocks is [REDACTED] throughout the simulated gas storage. Potential for [REDACTED] of salt in the roof was found to [REDACTED] in the finite difference model. Thus the [REDACTED] throughout gas storage service.

The finite difference modeling results indicate that the potential for [REDACTED]
[REDACTED] Some [REDACTED] in the cavern

CONTAINS PRIVILEGED INFORMATION
DO NOT RELEASE

walls is indicated by the model results. However, this [REDACTED] is not expected to

[REDACTED] Therefore the [REDACTED]

[REDACTED] The

[REDACTED] The extent of the [REDACTED] is confined to

[REDACTED] A great number of [REDACTED] and

[REDACTED] These three observa-

tions provide strong arguments for concluding that the [REDACTED]

- Development of the structural stratigraphy at the site based on existing literature and borehole geophysical logs.
- Development of cavern geometries based on sonar surveys.
- Characterization of rock properties.
- Characterization of the in situ temperature and stress states.
- Finite difference modeling of the initial cavern development, dewatering, and natural gas service.

- Extremely limited dilation (microfracturing) in the surrounding salt.
- Sufficiently high factors of safety to preclude the possibility of shear failure in the surrounding nonsalt layers.
- Limited areas in which the least-compressive principal stresses approach the tensile strengths of the nonsalt and salt beds.
- Acceptable rates of closure and surface subsidence.

67

CONTAINS PRIVILEGED INFORMATION
DO NOT RELEASE

[REDACTED] Previous
geomechanical analyses [Osnes and Eyermann, 1996] indicated that natural gas storage in
Gallery No. 1 would [REDACTED] Natural gas has been successfully
stored in Gallery No. 1 since that study. The current analyses indicate that the [REDACTED]

Also, because the [REDACTED]
[REDACTED]

8.0 REFERENCES

Birdwell, 1961. *International Salt Company, Well No. 31, Watkins Glen, Schuyler, NY.* Nuclear Log, prepared by Birdwell for International Salt Company, April.

Carmichael, R. S. (ed.), 1982. *Handbook of Physical Properties of Rocks, Volume II,* CRC Press, Inc., Boca Raton, FL.

Coker, A. K., 1993. "Program Calculates Z-Factor for Natural Gas," *Oil & Gas Journal*, pp. 74-75.

Hodge, D. S., R. Eckert, and F. Revetta, 1982. "Geophysical Signature of Central and Western New York," *Guidebook for Field Trips in Western New York, Northern Pennsylvania, and Adjacent Southern Ontario*, E. J. Buehler and P. E. Calkin (eds.), New York State Geological Association, 54th Annual Meeting, Amherst, NY.

Itasca Consulting Group, Inc., 1997. *FLAC^{3D}: Fast Lagrangian Analysis of Continua in 3 Dimensions*, Minneapolis, MN.

Jacobi, R. and J. Fountain, 1993. "The Southern Extension and Reactivations of the Clarendon-Lindon Fault System," *Géographie physique et Quaternaire*, Vol. 47, No. 2, pp. 285-302.

Jacoby, C. H., 1962. "International Salt Brine Field at Watkins Glen, New York," *Proceedings, Symposium on Salt*, A. C. Bersticker (ed.), Northern Ohio Geological Society, Inc., Cleveland, OH, pp. 506-520.

Jacoby, C. H., 1969. "Storage of Hydrocarbons in Cavities in Bedded Salt Deposits Formed by Hydraulic Fracturing," *Proceedings, 3rd Symposium on Salt*, A. C. Bersticker (ed.), Northern Ohio Geological Society, Inc., Cleveland, OH, pp. 463-469.

Kreidler, W. L., A. M. Van Tyne, and K. M. Jorgensen, 1972. *Deep Wells in New York State*, Bulletin Number 418A, New York State Museum and Science Service, University of the State of New York, Albany, NY.

Medley, A. H., 1993. *Review of Watkins Glen Brine Field*, prepared for Max Levy, Wilmington, DE, by A. H. Medley, Tulsa, OK, November.

Nieland, J. D., 1991. *SALT_SUBSID: A PC-Based Subsidence Model. User's Manual*, RSI-0389, prepared by RE/SPEC Inc., Rapid City, SD.

CONTAINS PRIVILEGED INFORMATION
DO NOT RELEASE

Norton, F. H., 1929. *Creep of Steel at High Temperatures*, McGraw-Hill Book Company, New York, NY.

Osnes, J. D. and T. J. Eyermann, 1996. *Geomechanical Analyses of Compressed Natural Gas Storage in Gallery No. 1, Watkins Glen, New York*, RSI-0670, prepared by RE/SPEC Inc., Rapid City, SD, for PB-KBB, Inc., Houston, TX.

PB-KBB, Inc., 1995. Personal communication between R. Blair, PB-KBB, Inc., Houston, TX, and T. J. Eyermann, RE/SPEC Inc., Rapid City, SD, November.

Pfeifle, T. W., 1996. *Mechanical Properties of Salt and Dolostone From Akzo Nobel Salt Inc. Well No. 58 and NYSEG Well No. 59, Seneca Lake Project, Watkins Glen, New York*, RSI-0668, prepared by RE/SPEC Inc., Rapid City, SD, for PB-KBB, Inc., Houston, TX.

Ratigan, J. L., L. L. Van Sambeek, K. L. DeVries, and J. D. Nieland, 1991. *The Influence of Seal Design on the Development of the Disturbed Rock Zone in the WIPP Alcove Seal Tests*, RSI-400, prepared by RE/SPEC Inc., Rapid City, SD, for Sandia National Laboratories, Albuquerque, NM.

Rickard, L. V., 1969. *Stratigraphy of the Upper Silurian Salina Group, New York, Pennsylvania, Ohio, Ontario*, Map and Chart Series Number 12, New York State Museum and Science Service, University of the State of New York, Albany, NY.

Van Tyne, A. M., 1983. "Natural Gas Potential of the Devonian Black Shales of New York." *Northeastern Geology*, Vol. 5, No. 3/4, pp. 209-216.

Vogt, T. J., 1995. *Coring Activities, NYSEG Well No. 59, Seneca Lake Storage Project, Watkins Glen, New York*, RSI-0655, prepared by RE/SPEC Inc., Rapid City, SD, for PB-KBB, Inc., Houston, TX.

